Zoological Journal of the Linnean Society, 2022, **XX**, 1–33. With 16 figures.

Neurocranial bones are key to untangling the sea cow evolutionary tree: osteology of the skull of *Sobrarbesiren cardieli* (Mammalia: Pan-Sirenia)

ESTER DÍAZ-BERENGUER[1,*], MIGUEL MORENO-AZANZA[1,2,3], AINARA BADIOLA[4] and JOSÉ IGNACIO CANUDO[1]

[1]*Grupo Aragosaurus-IUCA, Facultad de Ciencias, Universidad de Zaragoza, 50009 Zaragoza, Spain*
[2]*Geobiotec, Departamento de Ciências da Terra, Universidade Nova de Lisboa, 2829-526, Caparica, Portugal*
[3]*Espaço Nova Paleo, Museu da Lourinhã, Lourinhã, Portugal*
[4]*Departamento de Geología, Universidad del País Vasco/Euskal Herriko Unibertsitatea, 48940 Leioa, Spain*

Received 2 March 2021; revised 30 January 2022; accepted for publication 16 February 2022

The pan-sirenian *Bauplan* is conservative, probably owing to the constraints of adaptation to an aquatic lifestyle. Gathering morphological data from extinct forms is complex, resulting in poorly resolved phylogenies for stem pan-sirenians. Extant sirenians ossify the falx cerebri and the tentorium cerebelli, membranes of the dura mater of the brain attached to the parietal bone. Nevertheless, these ossifications are not present in some pan-sirenians. The basioccipital bone has received little attention in the literature except for establishing the relative age of individuals. Here, we present new cranial elements and a detailed description of the skull of *Sobrarbesiren cardieli*, a stem pan-sirenian from the Lutetian of Spain represented by eight individuals; we study its intraspecific variation and palaeoecological implications and explore the evolution of the endocranial structures and the basioccipital bone in pan-sirenians. Six new phylogenetic characters are added to the latest pan-sirenian dataset, resulting in a well-resolved topology where *Sobrarbesiren* is recovered close to the root, in a clade with *Prototherium* and *Eotheroides aegyptiacum*. The basioccipital bone and the ossified endocranial membranes have a phylogenetic signal, and the absence of such endocranial structures represents the plesiomorphic condition for pan-sirenians and is not diagnostic for the family Protosirenidae as previously believed.

ADDITIONAL KEYWORDS: basioccipital bone – Eocene – falx cerebri – internal occipital protuberance – marine mammals – palaeoecology – phylogeny – sea cows – Spain – systematics – tentorium osseum.

INTRODUCTION

Sirenia is a monophyletic order of mammals included in the superorder Afrotheria Stanhope *et al.*, 1998, a clade well supported by molecular and genomic data (Amrine-Madsen *et al.*, 2003; Murphy *et al.*, 2004; Springer *et al.*, 2015), which encompasses the extant placental mammals that originated in Africa: Tenrecoidea, Macroscelidea, Tubulidentata, Proboscidea, Hyracoidea and Sirenia (Tabuce *et al.*, 2008). Within this superorder, the sirenians, proboscideans and hyracoideans form the clade Paenungulata Simpson, 1945, which is also broadly accepted on the basis of chromosomal studies (e.g. Murphy *et al.*, 2004; Kellogg *et al.*, 2007; Pardini *et al.*, 2007). Morphological data also support the inclusion of the extinct groups Desmostylia and Embrithopoda in Paenungulata (Asher *et al.*, 2003; Gheerbrant *et al.*, 2005). Furthermore, McKenna (1975) proposed the mirorder Tethytheria, whose members would have evolved along the Tethyan coasts, composed of proboscideans, desmostylians and sirenians. Nevertheless, this group is subject to controversy based on genetic studies (e.g. Ozawa *et al.*, 1997; Amrine-Madsen *et al.*, 2003; Kellogg *et al.*, 2007; Pardini *et al.*, 2007; Springer & Murphy, 2007; Seiffert, 2007). Although there is a reasonable consensus concerning

*Corresponding author. E-mail: ester.berenguer@gmail.com

the phylogenetic relationships of the order Sirenia, the contents remain unclear, and various phylogenetic proposals exist, especially for the Eocene taxa.

Savage (1976) proposed the first cladogram of sirenians, but it was Domning (1994) who proposed the first character matrix for Sirenia, based entirely on skull characters. The character matrix created by Domning (1994) is the basis for almost all subsequent sirenian cladistic analyses, albeit with the addition of new characters or redefinitions of some of them (i.e. Bajpai & Domning, 1997; Domning & Aguilera, 2008; Vélez-Juarbe & Domning, 2014; Springer *et al.*, 2015; Domning *et al.*, 2017). The exception is the phylogenetic analysis by Sagne (2001a), in whose matrix more than half the characters are new.

The earliest studies classified pan-sirenians in four families (e.g. Simpson, 1945; Domning, 1994; Sagne, 2001a): Prorastomidae, which includes the basalmost forms *Prorastomus* Owen, 1855 and *Pezosiren* Domning, 2001a; Protosirenidae, which includes basal four-legged Eocene sirenians, such as *Protosiren* Abel, 1907 and *Ashokia* Bajpai *et al.*, 2009; Dugongidae, which includes all forms closer to the Recent sirenian *Dugong* Lacépède, 1799 and comprises most of the fossil forms; and Trichechidae, which includes the forms closer to the manatee, *Trichechus* Linnaeus, 1758, whose fossil record begins in the late Oligocene (Siegfried, 1965).

Nevertheless, all these traditional taxonomic ranks have proved to be problematic. In all the phylogenetic proposals, the 'prorastomids' are recovered as a paraphyletic group at the base of the tree. Also, the position and monophyly of protosirenids and dugongids are in constant question. Protosirenids have been recovered both as a paraphyletic group (e.g. Domning, 1994; Springer *et al.*, 2015; Balaguer & Alba, 2016) and as a monophyletic group (e.g. Velez-Juarbe *et al.*, 2012; Vélez-Juarbe & Domning, 2014; Díaz-Berenguer *et al.*, 2018), containing Trichechidae in some cases (e.g. Sagne, 2001b; Domning *et al.*, 2017) or forming a polytomy with all the other Eocene sirenians except 'prorastomids' (Velez-Juarbe & Wood, 2018). The dugongids have been recovered both as paraphyletic, including Trichechidae (Domning, 1994; Díaz-Berenguer *et al.*, 2018) and as monophyletic (Sagne, 2001a; Velez-Juarbe *et al.*, 2012; Springer *et al.*, 2015; Domning *et al.*, 2017). To address these incongruences in the classical taxonomy and the phylogeny, Vélez-Juarbe & Wood (2018) updated the definition of Sirenia to refer only to the crown clade composed of the last common ancestor of *Trichechus manatus* Linnaeus, 1758 and *Dugong dugon* Müller, 1776 and used the term 'Pan-Sirenia' to refer 'to the pan-stem clade that includes crown Sirenia'. In this proposal, Dugongidae and Trichechidae are defined as mutually exclusive clades in Sirenia, thus solving the problem of the paraphyly of Dugongidae and leaving most of the Eocene forms as stem pan-sirenians.

It is noteworthy that this definition of Sirenia and the term Pan-Sirenia were first used by O'Leary *et al.* (2013: supplementary material, table 4), who defined Sirenia as a node-based crown clade, being 'the least inclusive clade of *Trichechus manatus* and *Dugong dugon*', thus compatible with the definition of Vélez-Juarbe & Wood (2018), and defined Pan-sirenia as the total clade of Sirenia, including 'all species more closely related to *Trichechus manatus* than to any other living species'.

Phylogenetic analysis based on the characters of endocranial structures preserved in cranial endocasts has also been proposed (e.g. Furusawa, 2004; Orihuela *et al.*, 2019). Nevertheless, characters relating to these structures are absent in most comprehensive phylogenetic analyses except for the one undertaken by Sagne [2001a: character 37].

The falx cerebri and the tentorium cerebelli are membranous projections of the dura mater of the brain attached to the ventral surface of the parietal. The former separates the cerebral hemispheres, and the latter separates the upper surface of the cerebellum and the occipital lobes (Nojima, 1990). These membranes can ossify and may thus be preserved in skulls of extant and fossil taxa. The ossification of the falx cerebri is known as the bony falx cerebri, and that of the tentorium cerebelli as the tentorium osseum; they meet in the internal occipital protuberance. Among mammals, the bony falx cerebri and/or the tentorium osseum and/or the internal occipital protuberance are present in primates, marsupials, some cetaceans and extant sirenians, among others (Nojima, 1988). Among extant recent sirenians, the only exception is the hydrodamaline *Hydrodamalis gigas* Zimmermann, 1780, which became extinct in the 18th century and lacks these structures (Edinger, 1933). However, the bony falx cerebri, the tentorium osseum and the internal occipital protuberance are not present in all sirenian taxa in the fossil record. Abel (1928) described their absence in the Egyptian protosirenid *Protosiren fraasi* Abel, 1907, which was corroborated by the study of several cranial endocasts assigned to this taxon (Edinger, 1933) and of the endocranium of *Protosiren fraasi* using computed tomography (Gingerich *et al.*, 1994). Furthermore, Sickenberg (1934) proposed the absence of the bony falx cerebri, tentorium osseum and internal occipital protuberance as one of the main differences between *Protosiren fraasi* and the dugongid *Eotheroides aegyptiacum* Owen, 1875. Subsequent studies have shown that these endocranial structures are absent or poorly developed in the other protosirenid species (Domning & Gingerich, 1994; Domning *et al.*, 2017), whereas they tend to be present in 'dugongids' and trichechids

(e.g. Sickenberg, 1934; Pilleri, 1987; Domning, 1988; Sagne, 2001a; Domning & Aguilera, 2008; Voss & Hampe, 2017, among others). Nevertheless, Domning *et al.* (2017: 16) suggest that the absence or near-absence of these endocranial structures could be 'primitive relative to trichechids and dugongids' and not only characteristic of protosirenids, because these structures are rudimentary in the 'prorastomid' *Pezosiren portelli* Domning, 2001a.

The fusion of the basioccipital to the basisphenoid is a criterion applied to establish the relative age of extant and fossil sirenians (e.g. Pocock, 1940; Bajpai & Domning, 1997; Vélez-Juarbe & Domning, 2014; Voss & Hampe, 2017), but little attention has been paid to the morphology of the basioccipital bone, and descriptions in scientific papers are usually short and scarcely informative. Nevertheless, Díaz-Berenguer *et al.* (2018) proposed that some differences exist in the morphology of this bone among Eocene taxa when they described the Spanish taxon *Sobrarbesiren cardieli* Díaz-Berenguer *et al.*, 2018.

Sobrarbesiren is a medium-sized quadrupedal sirenian from the middle Eocene (Lutetian) of the southern Pyrenees (Huesca Province, Spain), known from cranial and postcranial elements including skulls, vertebrae, ribs and limb bones of several individuals at different ontogenetic stages. This fossil collection has given us a good idea of the overall appearance of this ancient animal (Díaz-Berenguer *et al.*, 2018, 2020). *Sobrarbesiren* has been proposed as the sister taxon of Dugongidae and Trichechidae (Díaz-Berenguer *et al.*, 2018) or as a member of the basal group Pan-Sirenia (Velez-Juarbe & Wood, 2018). *Sobrarbesiren cardieli* is a key taxon for understanding the evolution of pan-sirenians.

Here, we present an extensive description of the holotype and paratype skulls of *Sobrarbesiren cardieli* and new specimens ranging from perinatals to young adults, including a partly preserved subadult–adult skull, numerous skull fragments and isolated dental elements, which add to our knowledge of the cranial osteology of this basal pan-sirenian and to its intraspecific variation. Based on the assumptions mentioned above, three characters related to the endocranial structures of pan-sirenians and three characters related to the basioccipital bone are proposed, and a new phylogenetic proposal for pan-sirenians is put forward.

MATERIAL AND METHODS

Material

Twenty-nine cranial elements from at least eight individuals at different ontogenetic stages were studied. These consist of the holotype and paratype skulls of *Sobrarbesiren cardieli* and other cranial bones (*MPZ 2017/1*–6) briefly described by Díaz-Berenguer *et al.* (2018) and another 23 new specimens, including a partly preserved subadult–adult skull, numerous skull fragments and isolated dental elements. All the material is housed in Museo de Ciencias Naturales de la Universidad de Zaragoza (MPZ).

Most of the Eocene comparative taxa were studied first hand, including *Prorastomus sirenoides* Owen, 1855, *Pezosiren portelli*, *Protosiren sattaensis* Gingerich *et al.*, 1995, *Protosiren smithae* Domning & Gingerich, 1994, *Eotheroides lambondrano* Samonds *et al.*, 2009, *Eosiren libyca* Andrews, 1902, '*Halitherium*' *taulannense* Sagne, 2001b, *Prototherium veronense* de Zigno, 1875, '*Prototherium*' *intermedium* Bizzotto, 1983 and the Holocene sirenians *Hydrodamalis gigas*, *Dugong dugon* and *Trichechus manatus*. The other pan-sirenian taxa were studied from the literature. For detailed material and references used in this study, see the Supporting Information (Table S1).

Methods

The anatomical nomenclature used in this study is what is common for fossil pan-sirenians (e.g. Robineau, 1969; Domning & Pervesler, 2001; Domning, 2001a; Zalmout & Gingerich, 2012; Domning *et al.*, 2017). The muscle names and insertions are based on the study by Domning (1977a), unless otherwise mentioned. The skull and dental measurements are based on the description by Domning (1978) and subsequent expansions (e.g. Domning *et al.*, 2017).

Phylogenetic analyses were carried out using TNT v.1.5 (Goloboff & Catalano, 2016). An updated version of the matrix by Vélez-Juarbe & Wood (2018) was used and is provided in the Supporting Information (File S1) and can be downloaded from Morphobank (http://morphobank.org/permalink/?P3923). Details on the methodology and datasets used are covered in the 'Phylogenetic analysis' section.

Institutional abbreviations

BMNH, British Museum (Natural History), London (UK); **CGM**, Cairo Geological Museum, El Cairo (Egypt); **MB.MA.**, Museum für Naturkunde, Berlin (Germany); **MGP-PD**, Museum of Geology and Paleontology, University of Padua, Padua (Italy); **MNHN**, Muséum National d'Histoire Naturelle, Paris (France); **MPZ**, Museo de Ciencias Naturales de la Universidad de Zaragoza, Zaragoza (Spain); **RGHP**, Réserve Géologique de Haute Provence, Alpes de Haute Provence (France); **USNM**, US National Museum of Natural History, Washington, DC (USA).

Anatomical abbreviations

aa, anterior arm; **alc**, alisphenoid canal; **as**, alisphenoid; **bf**, bony falx cerebri; **bk**, basioccipital mid-ventral keel; **bo**, basioccipital; **bs**, basisphenoid; **C**^{1}, upper canine; **con**, mandibular condyle; **cp**, coronoid process; **eam**, external auditory meatus; **eo**, exoccipital; **eoc**, external occipital crest; **eop**, external occipital protuberance; **fce**, depression at usual location of bony falx cerebri; **fio**, infraorbital foramen; **fm**, foramen magnum; **fr**, frontal; **I**$^{1–3}$, upper incisors; **if**, incisive foramen; **ilc**, insertions for the longus capitis muscle; **iop**, internal occipital protuberance; **j**, jugal; **jpostp**, postorbital process of jugal; **jpre**, preorbital process of jugal; **l**, lacrimal; **lf**, lacrimal foramen; **lof**, lamina orbitalis of frontal; **M**$^{1–3}$, upper molars; **maf**, mandibular fossa; **mf**, mesorostral fossa; **mx**, maxilla; **n**, nasal; **nc**, nuchal crest; **oc**, occipital condyle; **P**$^{1–5}$, upper premolars; **p**, parietal; **pal**, palatine; **pe**, periotic; **pf**, perilymphatic foramen; **pgp**, postglenoid process; **pm**, promontory; **pmx**, premaxilla; **poa**, posterior arm; **pp**, pars petrosa; **pre**, presphenoid; **pt**, pterygoid; **rcd**, insertion of rectus capitis dorsalis muscle; **so**, supraoccipital; **sop**, supraorbital process of frontal; **sq**, squamosal; **sr**, sigmoidal ridge; **ssc**, insertion of semispinalis capitis muscle; **ta**, tympanic arch; **tc**, temporal crest; **tco**, temporal condyle; **tf**, temporal fossa; **to**, tentorium osseum; **tsul**, transverse sulcus; **tt**, tegmen tympani; **zps**, zygomatic process of squamosal.

Additional abbreviations

Ch., phylogenetic characters, following the number and descriptions of Vélez-Juarbe & Wood (2018); numbers in parentheses [e.g. Ch.3 (2)] refer to the character state.

SYSTEMATIC PALAEONTOLOGY

Class Mammalia Linnaeus, 1758

Superorder Afrotheria Stanhope *et al.*, 1998

Mirorder Tethytheria McKenna, 1975

Clade Pan-Sirenia O'Leary *et al.*, 2013 (*sensu* Vélez-Juarbe & Wood, 2018)

Sobrarbesiren cardieli Díaz-Berenguer *et al.*, 2018

Holotype: Complete skull of an adult individual (*MPZ 2017/1*) (Figs 1-12).

Paratype skull elements: An almost complete skull of a subadult individual (MPZ 2017/2), a nasal premaxillary process (MPZ 2017/3), an isolated ?I^{1} (MPZ 2017/4) and an isolated ?I^{3} (MPZ 2017/5).

Referred specimens: MPZ 2020/591, a subadult–adult skull, which lacks the supraoccipital, exoccipital, basicranium and dentition; MPZ 2020/592–594, juvenile isolated left frontals; MPZ 2020/595, juvenile isolated right frontal; MPZ 2020/596, fragment of the posterior midpart of a juvenile left frontal; MPZ 2020/597, anterior part of a juvenile left frontal; MPZ 2020/598 and MPZ 2020/599, juvenile supraoccipitals; MPZ 2020/600–602, left occipital condyles; MPZ 2020/603, incomplete right squamosal; MPZ 2020/604, juvenile right squamosal that lacks the dorsal cranial portion; MPZ 2020/605, fragments of a juvenile left squamosal; MPZ 2020/606, incomplete left jugal; MPZ 2020/607, right tegmen tympani; MPZ 2020/608, left ascending ramus of mandible; MPZ 2020/610, right ?P^{2}; MPZ 2020/611–612, left ?P$^{3–4}$; MPZ 2020/613, undetermined premolar; MPZ 2020/614, deciduous premolar.

Type locality and distribution: Known only from the Castejón de Sobrarbe-41 (CS-41) fossil site (Comarca de Sobrarbe, Huesca Province, Spain), which is located in the upper part of the Sobrarbe Fm (Ainsa Basin, South Pyrenean Basin) (Díaz-Berenguer *et al.*, 2018). Fossils come from a marly, silty level interpreted as the filling of a distributary channel in a deltaic plain.

Diagnosis sensu *Díaz-Berenguer* et al. *(2018):* Pan-sirenian, based on the following synapomorphies: retracted and enlarged external nares [Ch.8 (1)]; premaxilla contacts the frontals [Ch.9 (1)]; and a P$^{1–5}$–M$^{1–3}$ post-canine dental formula [Ch.155 (1)]; and characterized by the following combination of characters (autapomorphies indicated with an asterisk): upper dental formula 2.1.5.3 (I^{2} absent); pterygoid fossa present, extending above the level of the roof of the internal nares [Ch.102 (1)]; alisphenoid canal present [Ch.101 (0)]; basioccipital rectangular and elongated* [Ch.226 (1)] (Fig. 2C); acromion process of the scapula hook-shaped*, which extends slightly to the dorsal border of the glenoid fossa*; posterior iliac spine of the innominate bone present*; lateral iliac spine that appears abruptly on the lateral surface of the ilium with a flattened ventrolateral surface*.

Description and comparison

The description of the skull and dental elements of *Sobrarbesiren* is based on eight individuals at different ontogenetic stages. The holotype skull *MPZ 2017/1* is considered an adult because the basisphenoid–basioccipital suture is obliterated (erroneously interpreted by Díaz-Berenguer *et al.*, 2018), although M^{3} exhibits only slight wear. It is therefore likely to represent a young adult. In the paratype skull MPZ 2017/2, the basioccipital is not preserved; however, M^{3} is erupted but not worn and the specimen is thus considered a subadult individual. In contrast, the

posterior border of the zygomatic process is at the level of M^2, which is considered a feature of adults (Mitchell, 1973; Sagne, 2001a). Therefore, this skull probably pertains to an individual at the limit between the subadult and adult stages. In addition, MPZ 2017/2 is slightly smaller than *MPZ 2017/1* and MPZ 2020/591 (for measurements, see Supporting Information, Table S2). The skull MPZ 2020/591 is larger than the type skulls (Supporting Information, Table S2). Criteria based on the fusion of the skull bones are difficult to apply in this case owing to the preservation of the specimen. Moreover, criteria based on the dentition cannot be applied either. Nevertheless, on the basis of its size (Supporting Information, Table S2), it can be considered a subadult–adult individual.

Premaxilla: Both premaxillae are preserved in the type skulls *MPZ 2017/1* (holotype) and MPZ 2017/2 (paratype) and in the skull MPZ 2020/591 (Fig. 1; Supporting Information, Table S2). Furthermore, an isolated right nasal process of the premaxilla (MPZ 2017/3) has been recovered (Fig. 3; Supporting Information, Table S2). Specimen *MPZ 2017/1* preserves the most complete premaxillae, which are 178 mm (left premaxilla) and 184 mm (right premaxilla) in length, measured from the anterior edge of the symphysis to the posterior end of the nasal process. Each premaxilla is 64 mm in height at the level of I^3 and contains two incisor alveoli, for I^1 and I^3 [Ch.143 (0)]. The inferior border of the I^1 alveolus is broken in the type skulls, but this alveolus seems to be small. It is located at the anterior tip of the premaxilla and is less than half the length of the premaxillary symphysis [Ch.140 (0)]. The alveolus of I^3 lies at the posterior end of the premaxilla, slightly anterior to the premaxilla–maxilla suture. Its maximum diameter is 10 mm, but it is deformed by taphonomic lateromedial compression. In the paratype skull (Figs 2A, B, 3A, B), the alveolus of I^1 is 6 mm × 6 mm, but it is broken. The diameters of the I^3 and C^1 alveoli are 6 and 5 mm, respectively. The deflection of the masticating surface of the rostrum is ~32° from the occlusal plane, as measured in the holotype skull (*MPZ 2017/1*). The ventral part of the premaxilla is not preserved in the other skulls. The anterior edge of the rostrum is broad and flattened in anterior view and becomes narrower along the gently flattened dorsal border of the premaxillary symphysis to finish in a convex summit immediately anterior to the mesorostral fossa (Fig. 1: mf). The premaxillary symphysis is 105 mm in length in the most complete skull (*MPZ 2017/1*) and is enlarged relative to the cranium [Ch.3 (2)] and laterally compressed [Ch.10 (1)]. The ratio of the symphyseal length to the total length of the skull is ~3.5:1, and the rostral symphysis is more than half the total length of the premaxilla. The anteroventralmost end of the suture with the maxilla is on the vertical level of the symphyseal summit. The nasal process of the premaxilla is long, thin and tapering at the posterior end [Ch.6 (0)]. It is 79–82 mm long in *MPZ 2017/1*, 82 mm in MPZ 2017/2 and 90 mm in MPZ 2020/591, as measured from the anterior edge of the mesorostral fossa to the posterior edge of the nasal process, and it extends posteriorly less than one-third of the anteroposterior length of the supraorbital process. It is long (distance from rear of symphysis to posterior end of premaxilla more than half the length of the symphysis) [Ch.7 (0)]. The nasal process of the premaxilla is curved in lateral view, and its posterior edge expands slightly lateromedially. It is 24 mm wide in *MPZ 2017/1*, 19 mm in MPZ 2017/2 and 25 mm in MPZ 2020/591. The nasal process contacts the maxilla ventrally, the nasals posteromedially and the frontals posterolaterally. There is no contact with the lacrimal. The external nares are enlarged and retracted, as in all pan-sirenians [Ch.8 (1)]. The mesorostral fossa is long and narrow but is distorted by compression in all the skulls. Its anterior edge is rounded, and it is bounded anteriorly and laterally by the premaxillae and posteriorly by the nasals (at the level of the anterior orbital margin), with no contribution from the frontals.

The ventral/palatal surface of the premaxilla is deformed by compression in the skull *MPZ 2017/1*; it is not preserved in MPZ 2020/591, but it is well preserved in the skull MPZ 2017/2 (Fig. 2A, B). The incisive foramen is diamond-shaped and is bounded by the premaxillae laterally, anteriorly and dorsally, and by the maxillae posteriorly. It is ~20 mm in width and 21 mm long, and it opens downward. The rostral masticating surface is trapezoidal, and its maximum breadth is 48 mm at the level of I^3.

The isolated right nasal process of the premaxilla MPZ 2017/3 is 85 mm long (Fig. 3). The nasal branch is oval in cross-section and 9 mm in maximum diameter. The posterior end is diamond-shaped and dorsoventrally flattened, and it has a maximum mediolateral width of 19 mm. It is similar in size to the nasal process of the subadult–adult skulls; hence, it is considered to pertain to a subadult–adult specimen.

Nasal: Both nasals are preserved in the three studied skulls, but they are incomplete in MPZ 2020/591 (Fig. 4: n; Supporting Information, Table S2). The nasals are large and anteroposteriorly elongated, and they meet along their dorsomedial borders [Ch.31 (0)], as in 'prorastomids' (Savage *et al.*, 1994; Domning, 2001a), protosirenids (Sickenberg, 1934; Bajpai *et al.*, 2009; Domning *et al.*, 2017) except *Protosiren smithae* (Domning & Gingerich, 1994) and some other Eocene pan-sirenians, such as *Prototherium veronense* and *Eotheroides* spp. (Sickenberg, 1934; Samonds *et al.*, 2009; Zalmout & Gingerich, 2012). They are set in sockets in the anteromedial margin of the frontals. The nasals

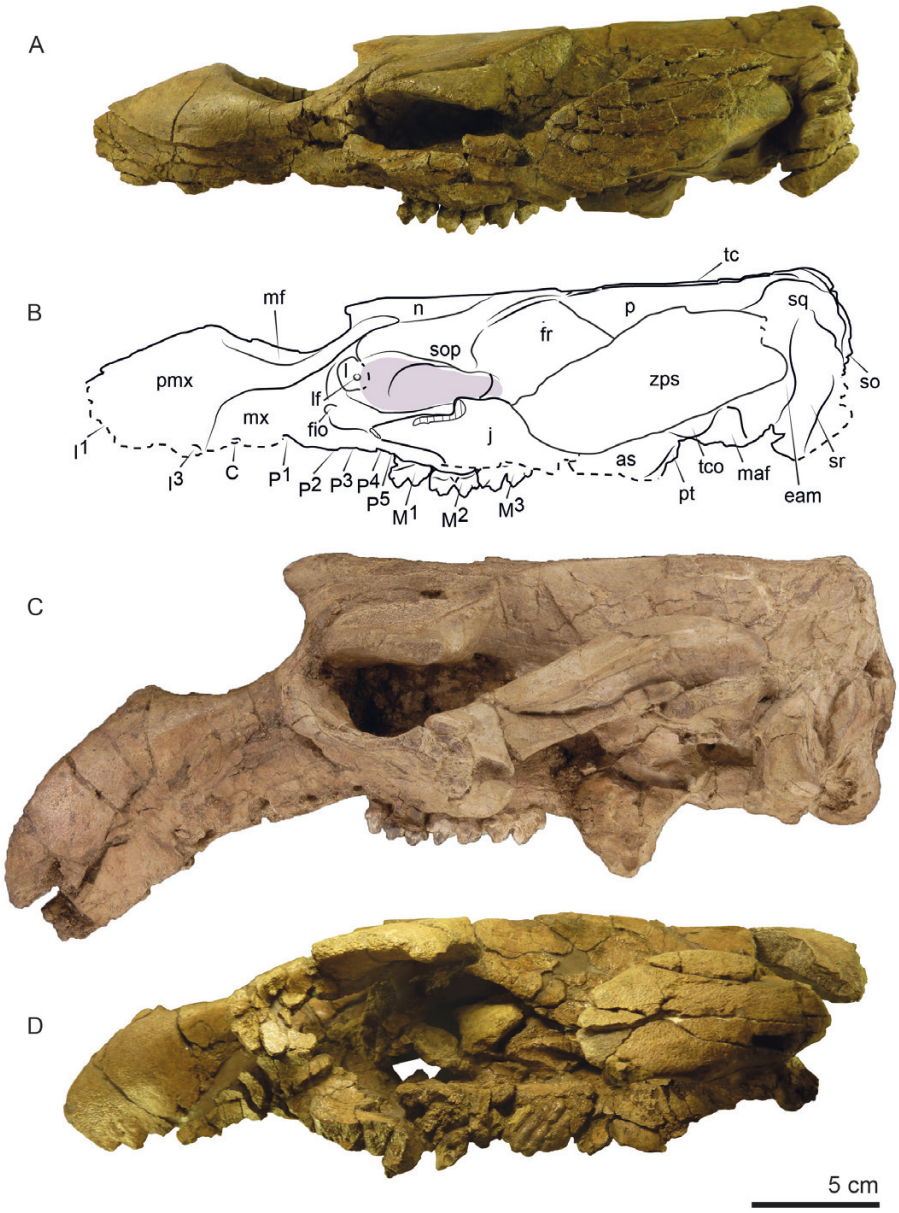

Figure 1. Skulls of *Sobrarbesiren cardieli* in lateral view. A, paratype skull MPZ 2017/2. B, interpretative sketch of the paratype skull. C, holotype skull *MPZ 2017/1*. D, skull MPZ 2020/591. Sutures are marked with continuous lines. Dashed lines indicate incomplete bones, and dashed areas denote broken surfaces. For abbreviations, see the Material and Methods section.

extend further than the anterior border of the orbit and are exposed dorsally on the skull roof for a total length of 70 mm in *MPZ 2017/1* and 61 mm in MPZ 2017/2. The anterior borders of the nasals are separated by a nasal incisure. Together, they form a V-shaped extension beyond the posterior edge of the mesorostral fossa [Ch.37 (0)]. Their dorsal surface is arched upward to reach a level higher than both frontals and parietals in *MPZ 2017/1*, but they are at the same level in MPZ 2017/2 and MPZ 2020/591 (Fig. 1). The elevation observed in *MPZ 2017/1* might therefore be attributable to the taphonomic lateromedial compression of this skull. The ratio of the maximum breadth of both nasals to their anteroposterior length is approximately one. The lateral side of the nasal shows an anterolateral constriction where it contacts the premaxillary nasal process, and its posterior edge is rounded. The nasals are shallowly separated by the frontals. The suture with the frontals is evidenced by interdigitations in MPZ 2017/2 and MPZ 2020/591 (Fig. 4A, B).

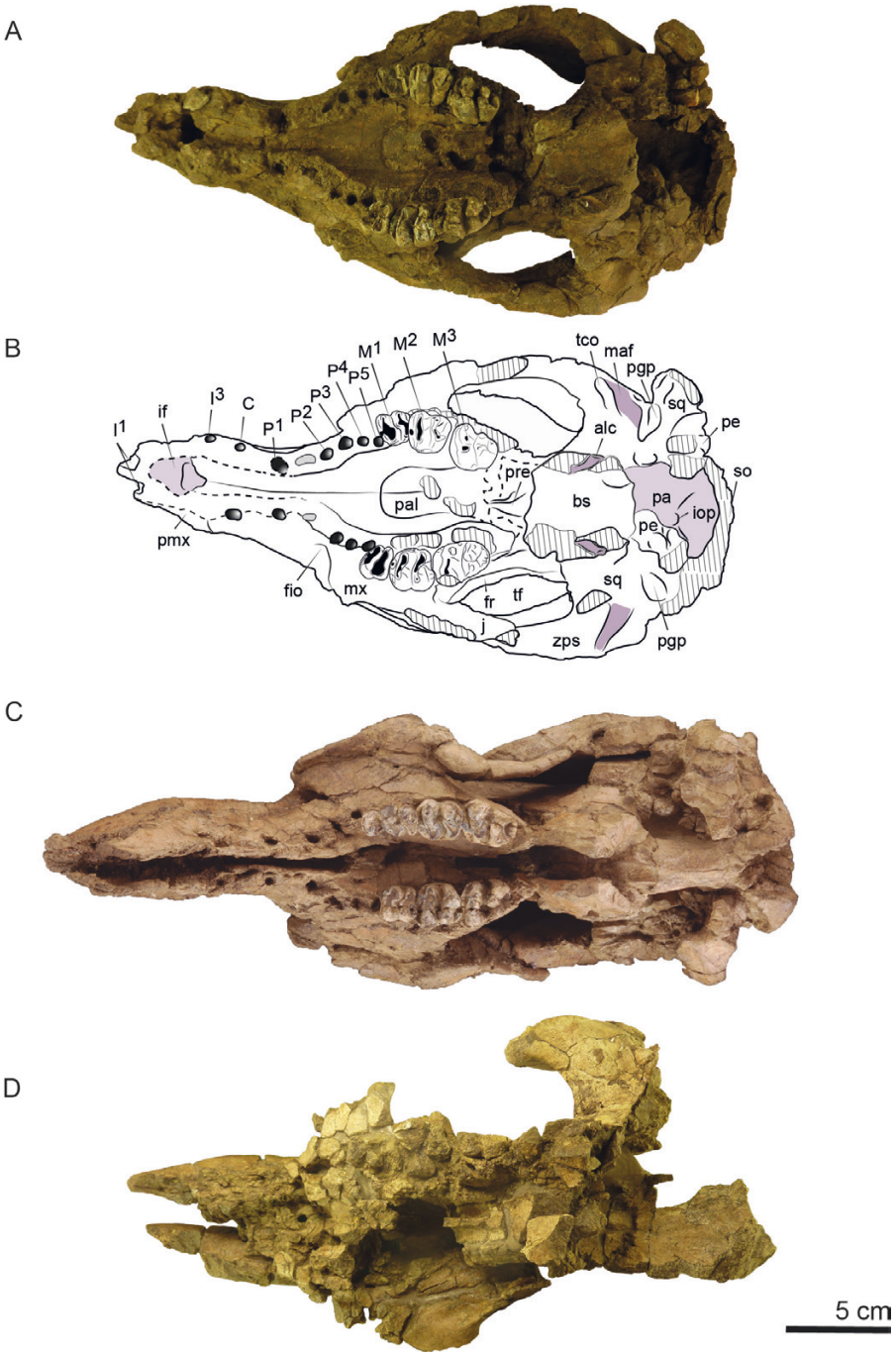

Figure 2. Skulls of *Sobrarbesiren cardieli* in ventral view. A, paratype skull MPZ 2017/2. B, interpretative sketch of the paratype skull. C, holotype skull *MPZ 2017/1*. D, skull MPZ 2020/591. Sutures are marked with continuous lines. Dashed lines indicate incomplete bones, and dashed areas denote broken surfaces. For abbreviations, see the Material and Methods section.

Vomer: The vomer (Fig. 4A, B: v) is well preserved only in the skull MPZ 2017/2. It is exposed in the mesorostral fossa. The vomer is elongated and lies above the dorsal surface of the maxillae. Dorsally, two thin laminae contact anteriorly, forming a narrow V, which extends to the anterior border of the mesorostral fossa. They delimit a U-shaped valley. Posteriorly, the bone narrows, and the laminae become closer.

Lacrimal: The lacrimals can be observed in the three skulls (Fig. 1: l), but they are only preserved in part. The lacrimal is a relatively large bone (≥ 16 mm in

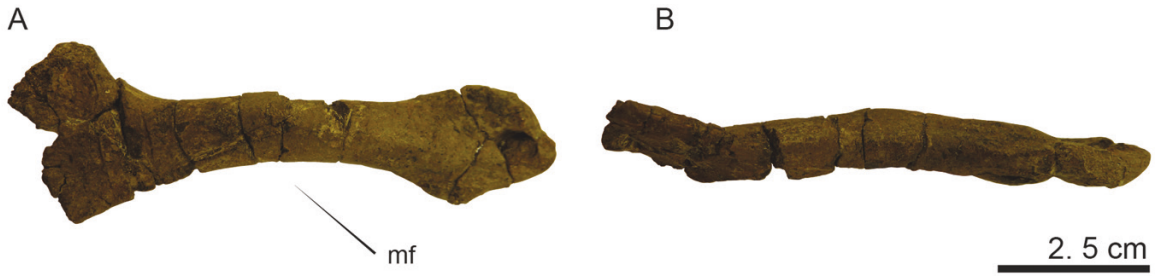

Figure 3. Isolated right nasal process of the premaxilla of *Sobrarbesiren cardieli* (MPZ 2017/3) in dorsal (A) and medial (B) views. For abbreviations, see the Material and Methods section.

anteroposterior width on the left side of the holotype skull *MPZ 2017/1*). Its anterior edge is rounded, but the posterior side is poorly preserved. The lacrimal faces posterolaterally and is surrounded by the maxillae ventrally and anterodorsally, forming the anteromedial border of the orbit, and by the supraorbital process of the frontal dorsally [Ch.93 (0)]. The lacrimal foramen (nasolacrimal canal; Fig. 1: lf) is small and opens laterally [Ch.91 (0)]. Tubercles or protuberances are absent.

Frontal: Both frontals are preserved in the type skulls and in the skull MPZ 2020/591 (Fig. 4: fr; Supporting Information, Table S2). Furthermore, four complete, isolated frontals are recovered (Fig. 5): MPZ 2020/592, MPZ 2020/593 and MPZ 2020/594 are left frontals, and MPZ 2020/595 is a right frontal. In addition, MPZ 2020/596 is a fragment of the posterior midpart of a left frontal, and MPZ 2020/597 is the anterior part of a left frontal. All these isolated specimens are assigned to perinatal to juvenile individuals because of their small size. The frontals form the anterior midpart of the skull roof and contact the premaxilla anteromedially and the nasal medially (Fig. 4). The frontal roof of *Sobrarbesiren* is short relative to the parietals (i.e. interfrontal suture vs. length of parietals), as in 'prorastomids', protosirenids and *Eotheroides aegyptiacum*, *Prototherium ausetanum* Balaguer & Alba, 2016 and '*Halitherium*' *taulannense* (Domning & Gingerich, 1994; Savage *et al.*, 1994; Sagne, 2001a; Bajpai *et al.*, 2009; Balaguer & Alba, 2016; Domning *et al.*, 2017), and in contrast to some other Eocene pan-sirenians, such as *Prototherium veronense*, *Eotheroides clavigerum* Zalmout & Gingerich, 2012, *Eotheroides sandersi* Zalmout & Gingerich, 2012 and *Eosiren stromeri* Abel, 1913 (Domning, 1994; Zalmout & Gingerich, 2012: table 3). The frontals are flat between the temporal crests [Ch.42 (0)] (Fig. 4: tc) and do not bear knoblike bosses [Ch.45 (0)]. Their lateral walls are narrowed posteriorly at the anterior edge of the frontoparietal suture. The supraorbital processes (Fig. 4: sop) of the frontals are stout, dense and dorsoventrally flattened, 10–15 mm thick and show a prominent posterolateral corner [Ch.36 (0)]. Their lateral borders are not divided [Ch.44 (0)]. They reach the posterior end of the nasals. The almost straight posterior border of the supraorbital process shows a blunt bulge, which is present in the type skulls and in the skull MPZ 2020/591. In addition, the holotype and paratype skulls show several cord-like protuberances on the dorsal edge of the posterolateral corner of the frontal, immediately before the beginning of the frontoparietal suture. These cords are directed anteromedially to posterolaterally and increase in length distally. They are more marked in the holotype skull than in the paratype. The anterolateral border of the supraorbital process shows a rugose texture. The dorsolateral surface of the frontals is distinctly demarcated by low and blunt temporal crests, which are oriented anterolaterally to posteromedially. The beginning of the frontoparietal suture is marked by a dorsolateral prominence. Posteriorly, the frontoparietal suture is V-shaped. The ratio of the maximum breadth across the supraorbital processes to the maximum length of the frontals is 1.7. The lateral edges of the frontals are sharp and overhanging. The lamina orbitalis of the frontal is covered by sediment in the holotype skull *MPZ 2017/1* and is not visible in the paratype skull MPZ 2017/2 because the orbits are collapsed. However, it is well preserved in the left frontal of the skull MPZ 2020/591 and is preserved, in part, in the isolated juvenile frontal MPZ 2020/593 (Fig. 5B, E). This lamina forms a thin wall (6 mm in thickness in MPZ 2020/591 and 3 mm in MPZ 2020/593). An orbitotemporal crest is absent. The frontals contact the parietals posteriorly and the alisphenoid ventrally.

Juvenile frontals: The general morphology of the isolated juvenile frontals (Fig. 5) is similar to that of the subadult skulls. The left and right frontals MPZ 2020/593 and MPZ 2020/595 are similar in size, whereas MPZ 2020/592 and MPZ 2020/594 are smaller (Fig. 5; Supporting Information, Table S2). The most anterior edge of the frontals shows a slightly concave surface inclined medially for the contact with the premaxilla (Fig. 5D). The specimens MPZ 2020/593 and MPZ 2020/595 show well-developed supraorbital processes, whereas these processes are small, and almost indistinguishable in dorsal view, in the younger specimens MPZ 2020/592

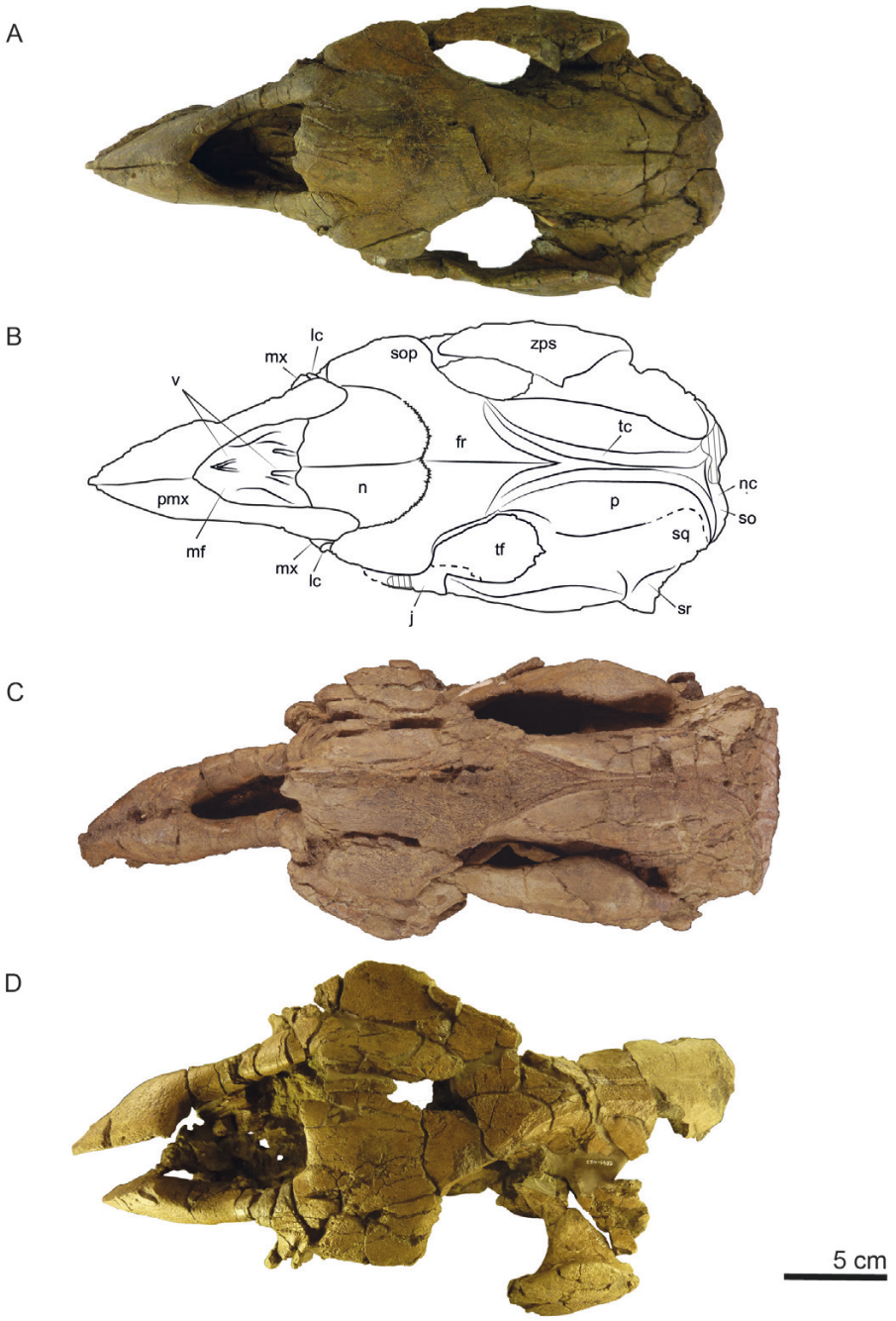

Figure 4. Skulls of *Sobrarbesiren cardieli* in dorsal view. A, paratype skull MPZ 2017/2. B, interpretative sketch of the paratype skull. C, holotype skull *MPZ 2017/1*. D, skull MPZ 2020/591. Sutures are marked with continuous lines. Dashed lines indicate incomplete bones, and dashed areas denote broken surfaces. For abbreviations, see the Material and Methods section.

and MPZ 2020/594, and the lateral side of the frontal is almost flat, without the usual lateral deviation of the frontal (Fig. 5G–L). The medial side of the frontal, where it contacts the nasal bone, is a thin lamina, which overhangs the nasal cavity. Posteriorly, the medial side shows a thick, sickle-shaped, rugose vertical surface where the two frontals contact. In specimens MPZ 2020/592 and MPZ 2020/594, this surface is reduced in size and smoother than in the specimens MPZ 2020/593 and MPZ 2020/595.

The ventral surface of the frontals is occupied by several deep and elongated concavities. These

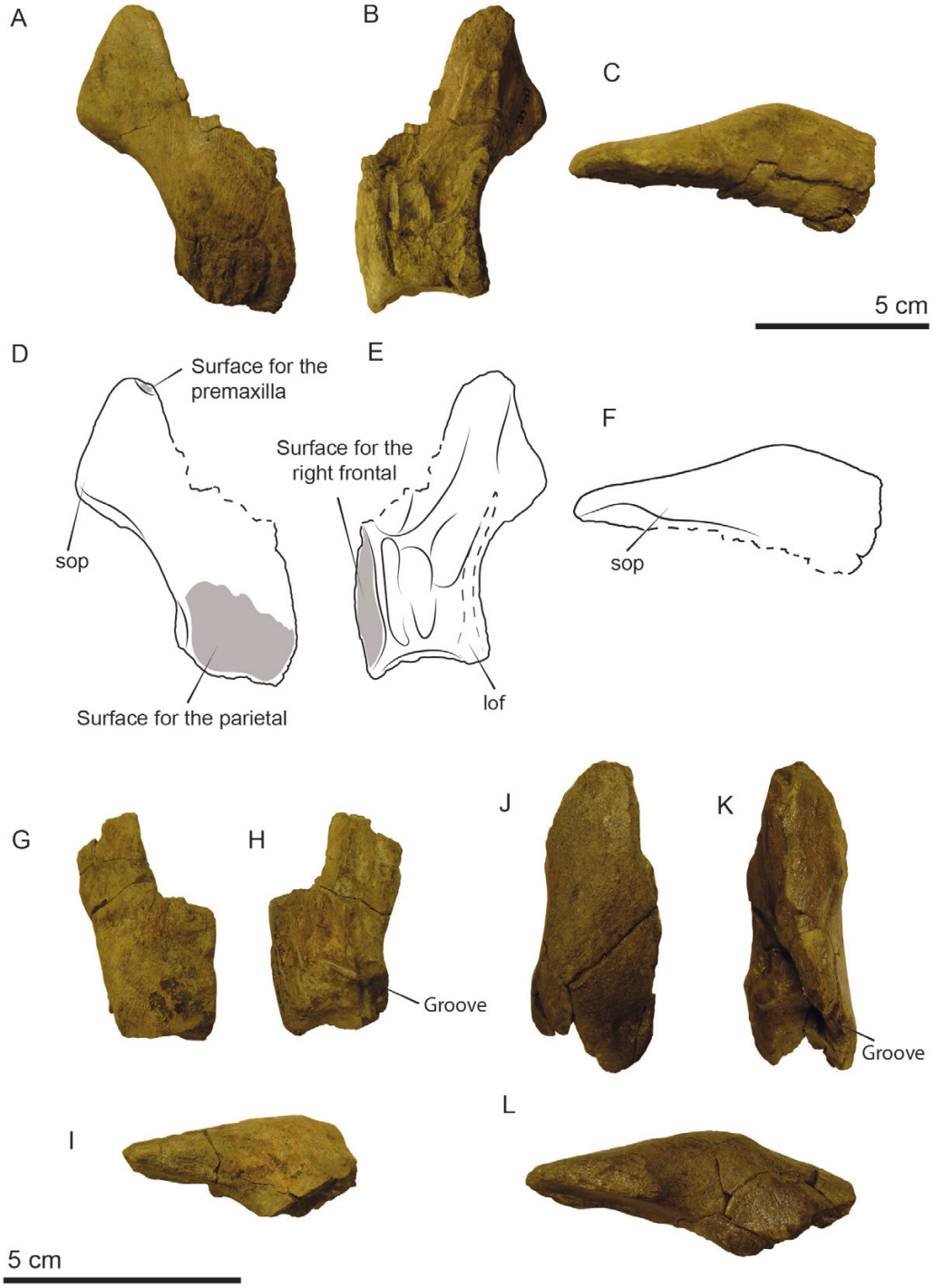

Figure 5. Frontal bones assigned to immature individuals of *Sobrarbesiren cardieli*. A–F, MPZ 2020/593, left frontal in dorsal (A), ventral (B) and lateral (C) views, and interpretative sketches (D–F, respectively). G–I, MPZ 2020/592, left frontal in dorsal (G), ventral (H) and lateral (I) views. J–L, MPZ 2020/594, left frontal in dorsal (J), ventral (K) and lateral (L) views. Dashed lines indicate incomplete parts. For abbreviations, see the Material and Methods section.

structures seem to be absent or poorly developed in other sirenians, such as *Metaxytherium krahuletzi* Depéret, 1895 (Domning & Pervesler, 2001: plates 1, 2b), *Metaxytherium serresii* Gervais, 1847 (Carone & Domning, 2007: plates 1b, 3), and *Eotheroides sandersi* (Zalmout & Gingerich, 2012: fig. 43), in which the

ventral side of the frontal is a plane surface. The frontals reach their maximum thickness at their posterior midpart (17–22 mm), whose dorsal surface is inclined posterolaterally; this sutural surface is irregular and covered with longitudinal grooves, where the parietals contact this bone. The posteroventral side of the frontals (i.e. the anterior border of the cranial cavity) is a suboval, smooth and concave surface. Both the contact surface with the parietals and the concavities on the ventral surface of the frontals are less marked and subtler in MPZ 2020/592 and MPZ 2020/594 than in the other juvenile frontals. Both MPZ 2020/592 and MPZ 2020/594 are proportionally shorter anteroposteriorly than the other specimens, although thick. Moreover, there is a deep transverse groove between the lateral wall of the frontal and the rest of the bone (Fig. 5K, L), which turns medially towards the medial wall of the frontal. Both MPZ 2020/592 and MPZ 2020/594 are thus interpreted as perinatal specimens because of their size and the fact that they are less developed.

Parietal: The parietals are well preserved in the type skulls (*MPZ 2017/1* and MPZ 2017/2), and the dorsal part of the parietals is preserved in the skull MPZ 2020/591 (Fig. 4B: p; Supporting Information, Table S2). The parietals form the posterior midpart of the skull roof. They cover a length of 88 mm of the *MPZ 2017/1* skull roof, 57 mm in the skull MPZ 2017/2 and > 74 mm in the skull MPZ 2020/591, less than the nasal–frontal portion of the skull (135 mm in *MPZ 2017/1*, 115 mm in MPZ 2017/2 and 120 mm in MPZ 2020/591). The parietal portion is slightly longer than the frontal portion (length of interfrontal suture: 58 mm in *MPZ 2017/1*, 57 mm in MPZ 2017/2 and 59 mm in MPZ 2020/591). The parietals are elongated and convex bones. The frontal processes exceed half of the interfrontal length in the type skulls and in the skull MPZ 2020/591 (estimated). Thus, they are long, as in *Prototherium veronense* and '*Halitherium*' *taulannense*, unlike other Eocene pan-sirenians (Sagne, 2001a: Ch.20). The interparietal suture and the parieto-occipital sutures are completely closed and cannot be distinguished in any of the subadult–adult specimens studied. The parietals show smooth temporal crests that begin in the anterior and lateral contacts of the frontoparietal suture; thus, these crests are marked in both the frontal and the parietal, as in other Eocene pan-sirenians except *Prorastomus*, with temporal crests limited to the frontal bone (Savage *et al.*, 1994), and *Libysiren sickenbergi* Domning *et al.*, 2017, with temporal crests limited to the posterior part of the parietals. The temporal crests show variability between the different specimens. In the holotype, they are thin and join immediately behind the frontoparietal suture for a total of 52 mm in anteroposterior length. They join immediately behind the frontoparietal suture in the skull MPZ 2020/591 for a total length of 40 mm, but in this specimen the crests are wider, resulting in a more flattened vault in its more dorsal part. In the paratype, the temporal crests are wider than in the holotype and separated 3 mm from one another (Fig. 4A, B). The smooth temporal crests of *Sobrarbesiren* differ from all other Eocene pan-sirenians, except the 'prorastomid' *Pezosiren*, in being joined, or nearly so, in the parietals. Nevertheless, the temporal crests of *Sobrarbesiren* are not raised, unlike in *Pezosiren*. Thus, a true sagittal crest is absent in all the specimens [Ch.51 (1)]. Posteriorly, the temporal crests separate before reaching the nuchal crest and delimit a shallow triangular depression. Three emissary foramina forming a triangle are situated in this depression in the holotype skull, but they are absent in the paratype skull. The parietal bone has a dorsoventral thickness of 29 mm in the skull MPZ 2020/591.

Endocranial structures: The endocranial structures can be observed in the paratype skull MPZ 2017/2, in the skull MPZ 2020/591 and in the isolated juvenile skullcaps MPZ 2020/598 and MPZ 2020/599 (Fig. 6). The bony falx cerebri (Fig. 6: fce) is absent in all the studied specimens [Ch.223 (1)]. Instead of it, there is a shallow groove along the interparietal suture (Fig. 6A, E), which transforms into a deep groove between the frontals. A low tentorium osseum (Fig. 6: to) and shallow transverse sulci directed posterolaterally (Fig. 6: tsul) are present in MPZ 2017/2 and in MPZ 2020/598 [Ch.224 (1)], but are less marked in the latter. These structures are less marked in the skull MPZ 2020/591. In addition, the ventral surface of the supraoccipital is covered by small pits in the specimen MPZ 2020/598 (Fig. 6C–F). A blunt internal occipital protuberance (Fig. 6: iop) is present in all the specimens [Ch.225 (1)]. Thus, *Sobrarbesiren* lacks a bony falx cerebri, like protosirenids and *Pezosiren* (see Fig. 13B, fce), but possesses the tentorium osseum and the internal occipital protuberance, unlike 'prorastomids' and protosirenids, although a low tentorium osseum is present in some specimens (Sickenberg, 1934; Domning & Gingerich, 1994; Gingerich *et al.*, 1994; Domning *et al.*, 2017).

Supraoccipital: The supraoccipital is complete but distorted in the holotype skull *MPZ 2017/1* (Fig. 7: so; Supporting Information, Table S2). In the paratype skull MPZ 2017/2, it is preserved only in its dorsal midpart (Fig. 7A, B). Furthermore, in the juvenile skullcaps MPZ 2020/598 and 599, the supraoccipital is almost complete (Fig. 6C–F; Supporting Information, Table S2). The supraoccipital contributes to the most posterior part of the skull roof. The general morphology and the relationship between the dorsal and ventral width of this bone are not clear in the holotype skull. The

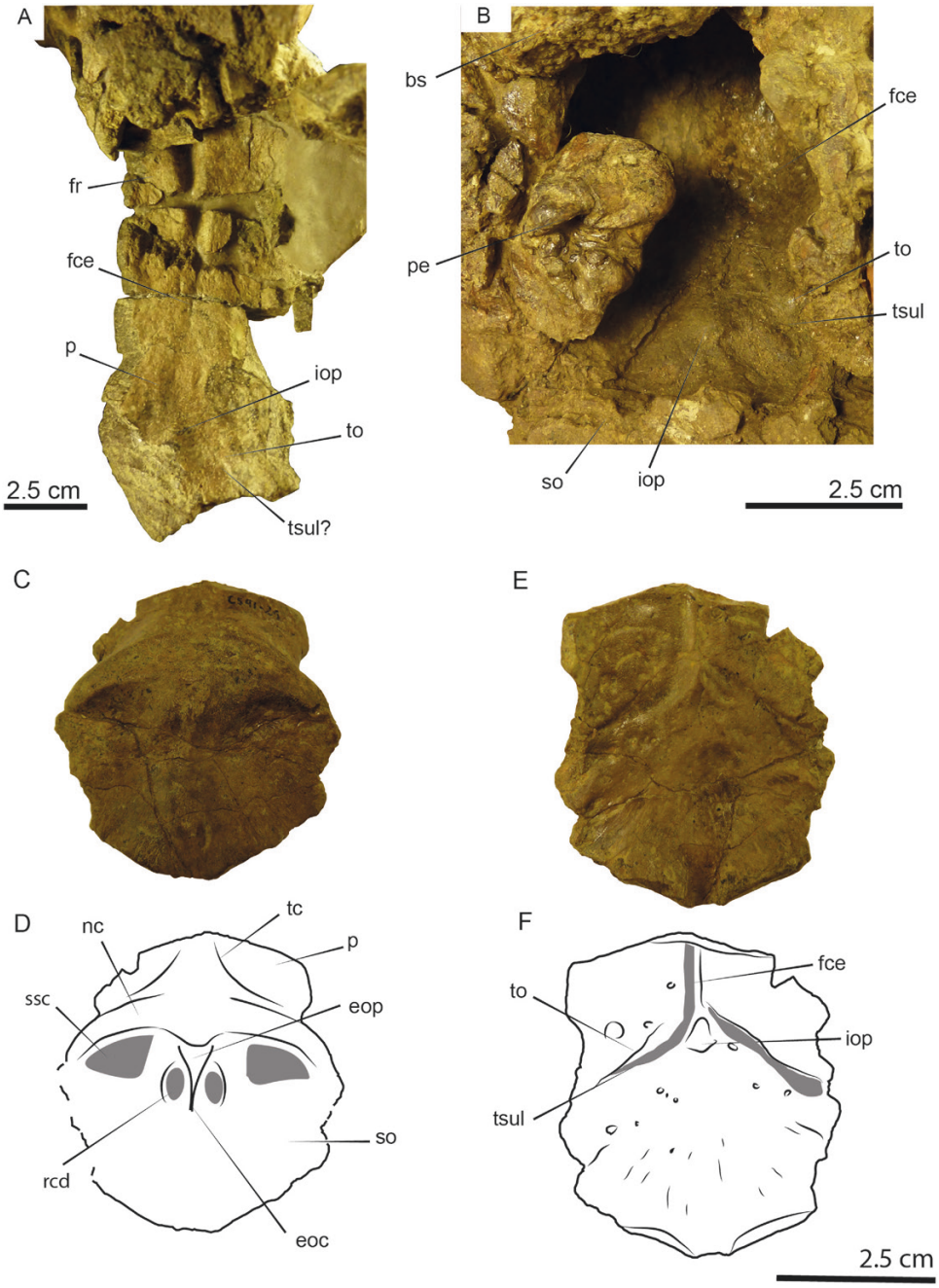

Figure 6. Endocranial structures of *Sobrarbesiren cardieli*. Skull roof of skull MPZ 2020/591 (A) and MPZ 2017/2 (B) in ventral view. C–F, MPZ 2020/598, parietal–supraoccipital skullcap of a juvenile individual in posterior (C) and ventral (E) views, and interpretative sketches (D, F, respectively). For abbreviations, see the Material and Methods section.

nuchal planum is bipartite owing to a weak and short median ridge, evident in the holotype and paratype skulls. This ridge separates the oval concavities for the rectus capitis dorsalis muscle insertions (Fig. 7: rcd), situated near the dorsal border of the bone. Lateral to these concavities there are two other paired concavities, bigger and deeper, surrounded dorsally by the nuchal crest (Fig. 6: nc), interpreted as the points of insertion of the semispinalis capitis muscles (Fig. 7: ssc). The external occipital protuberance (Fig. 7: eop) is a blunt triangular boss situated on the dorsal edge of the supraoccipital. The supraoccipital shows a pronounced nuchal crest positioned at the same level as the skull roof, semicircular in shape, curved laterally and lacking rugosities, but less massive than in protosirenids (Domning & Gingerich, 1994;

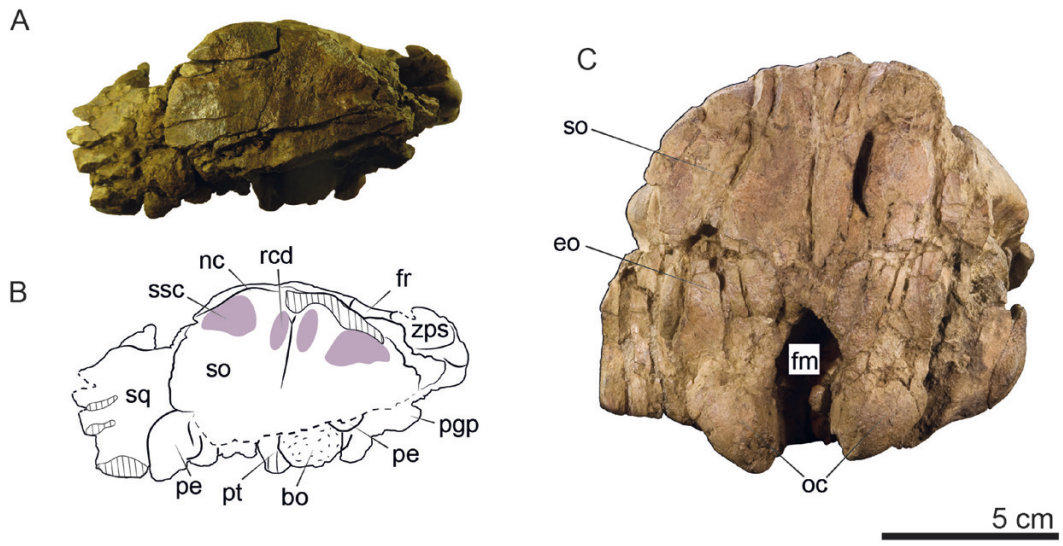

Figure 7. Skulls of *Sobrarbesiren cardieli* in posterior view. A, paratype skull MPZ 2017/2. B, interpretative sketch of the paratype skull. C, holotype skull *MPZ 2017/1*. Sutures are marked with continuous lines. Dashed lines indicate incomplete bones, and dashed areas denote broken surfaces. For abbreviations, see the Material and Methods section.

Bajpai *et al.*, 2009; Domning *et al.*, 2017). The supraoccipital forms an angle of 105° with the parietal in the holotype skull *MPZ 2017/1* and 100° in the paratype skull MPZ 2017/2, but both are distorted by fossil-diagenetic compression.

Juvenile parietal–supraoccipital skullcaps: The general morphology of the specimens MPZ 2020/598 and 599 is similar to that of the holotype and paratype skulls, but it is better preserved (Fig. 6C–F; Supporting Information, Table S2). The supraoccipital–parietal suture is almost obliterated but still discernible. The supraoccipital is wider in its dorsal half than at the ventral extremities of the lateral borders [Ch.64 (0)], as in the other Eocene pan-sirenians (Domning *et al.*, 2017; Springer *et al.*, 2015: Ch.64). Its outline is hexagonal, and it has a relatively flat posterior surface. The external occipital protuberance is a small blunt boss on the dorsal part of the supraoccipital and, immediately below it, there is a short median ridge limited to the dorsal half of the bone. The concavities for the insertion of the semispinalis capitis muscles (the lateral, bigger ones) and the rectus capitis dorsalis muscles (the medial, smaller ones) are also present. The posterior surface of the supraoccipital forms an angle with the dorsal plane of the skull roof of 138° in MPZ 2020/598 and 130° in MPZ 2020/599. In ventral view, the ventral border of the supraoccipital is V-shaped and divided by a narrow furrow into two suboval surfaces for the fusion with the exoccipital.

Exoccipitals: The exoccipitals are preserved only in the holotype skull *MPZ 2017/1* (Fig. 7: eo; Supporting Information, Table S2). The lateromedial compression of the skull has obscured the original morphology. Three isolated left occipital condyles, MPZ 2020/600–602, are also preserved. The exoccipitals are connected along a midline suture, 11 mm in length, dorsal to the foramen magnum [Ch.66 (0)], as in all the Eocene pan-sirenians except *Protosiren smithae* (Domning & Gingerich, 1994). The ratio of the maximum exoccipital height to the maximum exoccipital breadth is 0.58, and the breadth of the exoccipitals is 87 mm. The foramen magnum (Fig. 7: fm) is oval, with its dorsal border pointed, probably distorted by the lateromedial compression, with a height that exceeds its width. The dorsolateral borders of the exoccipital are rounded and smooth [Ch.70 (1)]. The supraoccipital–exoccipital suture is not well preserved in the holotype skull. Nevertheless, the ventral border of the complete juvenile supraoccipital MPZ 2020/598 shows that this suture was V-shaped (Fig. 6C, D). The presence of supracondylar fossae above the condyles is not clear, but if they were present, they would have been shallow and located directly above the dorsal part of the condyle [Ch.67 (0,1)], as in 'prorastomids' and protosirenids (Domning & Gingerich, 1994; Savage *et al.*, 1994; Domning *et al.*, 2017), except *Ashokia* Bajpai *et al.*, 2009.

The occipital condyles are kidney-shaped, wide dorsally and narrowing ventrally. They are 25 mm apart at their bases in *MPZ 2017/1* and curved almost vertically (Fig. 7C), as in the other Eocene pan-sirenians, except *Pezosiren* (specimen USNM 553590). The paraoccipital processes are almost at the same ventral level as the condyles and are separated

by 11 mm from them. These processes have blunted, curved ends to accommodate the periotic along with the squamosal. The presence of hypoglossal foramina is not clearly discernible [Ch.72 (?)]. The exoccipitals contact the supraoccipital dorsally, the basioccipital ventrally and the squamosal laterally.

Basioccipital: The basioccipital is preserved only in the holotype skull *MPZ 2017/1*. The basioccipital–basisphenoid suture is completely closed. The basioccipital is 38 mm long (from the line of fusion with the basisphenoid to the base of the foramen magnum) and 17.5 mm wide. It is elongated and almost rectangular in ventral view, maintaining the same width along its body [Ch.226 (1)] (Fig. 2C; see Phylogenetic analysis section), unlike the basioccipital of the rest of the pan-sirenians. The basioccipital is transversely wider posteriorly in 'prorastomids' (Savage *et al.*, 1994; basicranium USNM 553590 of *Pezosiren portelli*, and it is wasted in protosirenids and other pan-sirenians (see Phylogenetic analysis section). The anterior edge of the basioccipital of *Sobrarbesiren* is slightly more elevated than the posterior one. In ventral view, there are two symmetrical, shallow, elongated and smooth depressions for the insertion of the longus capitis muscles [Ch.227 (0)], as in *Prorastomus*. These depressions are deeper in other Eocene pan-sirenians, such as *Pezosiren* (basicranium USNM 553590), *Eotheroides aegyptiacum* (Abel, 1913: table (II) XXXI, 2) and '*Halitherium*' *taulannense* (see Phylogenetic analysis section). Protosirenids and most dugongids show convex rugosities on the basioccipital, instead of concavities, for the attachment of the longus capitis muscles (e.g. Domning, 1978, 1988; Bajpai *et al.*, 2009; Vélez-Juarbe & Domning, 2015; Voss & Hampe, 2017; Domning *et al.*, 2017). The depressions for the insertions of the longus capitis muscles of *Sobrarbesiren* are separated by a median keel, as in *Pezosiren*, *Prorastomus* and *Eotheroides aegyptiacum* (Savage *et al.*, 1994; basicranium USNM 553590 of *Pezosiren portelli*; Abel, 1913: table (II) XXXI, 2). This keel is shorter in *Eotheroides aegyptiacum* than in *Sobrarbesiren* and the 'prorastomids', but it bifurcates before the basioccipital–basisphenoid contact, as in *Sobrarbesiren*. Moreover, the ventral surface of the basioccipital is depressed between the rami of the keel in both taxa. Posteriorly, the keel extends almost to the foramen magnum [Ch.228 (0)].

Basisphenoid: The basisphenoid is preserved in the holotype skull *MPZ 2017/1* and partly preserved in the paratype skull MPZ 2017/2 (Fig. 2A–C: bs). The basisphenoid is a flattened and short bone in ventral view (46 mm in length in the paratype skull). It is inclined anterodorsally towards its contact with the presphenoid (Fig. 2A, B: pre). Its posterior part, immediately anterior to the basisphenoid–basioccipital suture, shows two low keels that delimit a shallow depressed area in the holotype skull, but these structures are not preserved in the paratype skull. Lateral to these rami, there are two concavities on the left and right sides, which occupy the most lateral posterior corners of the basisphenoid above the pterygoid fossa. The sutures with the pterygoid and the surrounding sphenoid bones are not clear in the type skulls. In the paratype skull the posterior contact surface with the basioccipital is exposed. It is pentagonal and rugose.

Presphenoid: The presphenoid is partly exposed between the broken palatines and the basisphenoid in the paratype skull MPZ 2017/2 (Fig. 2A–C), and it is partly preserved in the skull MPZ 2020/591. The presphenoid forms an elongated median crest. This crest gets higher towards the nasal cavity and reaches its maximum height (14 mm) in its anterior part, although it is incomplete. The sutures between the presphenoid and the surrounding bones are not visible, but it clearly contacts the basisphenoid posteriorly.

Orbitosphenoid: Not preserved.

Alisphenoid: The alisphenoids are well preserved in the holotype skull *MPZ 2017/1* (Fig. 1: as). In the paratype skull MPZ 2017/2, only the dorsal part is still present. In MPZ 2020/591, a fragment of the alisphenoid is articulated with a left squamosal, both associated with the skull MPZ 2020/591. The alisphenoids form the lateral side of the pterygoid processes, which are broken and inclined inward. Their bases are separated by an estimated distance of 45 mm measured between their lateral sides. The alisphenoid contacts the basisphenoid dorsomedially and the pterygoids medially. The dorsolateral contact with the squamosal is straight and located at the base of the medial wall of the temporal fossa. This contact is clearly visible on the left squamosal of the skull MPZ 2020/591. An alisphenoid canal (Fig. 2A, B: alc) is present [Ch.101 (0)], as in 'prorastomids' and protosirenids (Domning & Gingerich, 1994; Gingerich *et al.*, 1994; Savage *et al.*, 1994; Domning, 2001a; Domning *et al.*, 2017). It is exposed in the lateral surface of the alisphenoid in the holotype skull because the alisphenoids are broken and out of place, and in the ventral view of the paratype skull because the wings of the alisphenoid are not preserved. This canal is large (≥ 16 mm in length) in MPZ 2017/2. Its posterior opening is located in the lateral side of the alisphenoid, but its anterior opening is not clear in this skull. The foramen ovale is converted into an open notch [Ch.103 (1)].

Pterygoid: Like all non-'prorastomid' sirenians, *Sobrarbesiren* has a short sphenopalatine region, with

an enlarged pterygoid process (Domning, 2001a). The pterygoids are preserved in the specimen *MPZ 2017/1*, but they are broken at their roots and inclined inward. Their dorsal part is preserved in the paratype skull MPZ 2017/2 (Fig. 2: pt). The medial walls of the pterygoids are separated by an estimated distance of 36 mm at their base. These medial walls project further posteriorly than the lateral walls and converge dorsally at the posterior corner of the basisphenoid. The lateral side of the pterygoid presents a shallow, longitudinal groove immediately anterior to the posterior edge. The pterygoid constitutes the medial lamina and the posterior facet of the pterygoid process, which is enlarged, thickened and dorsoventrally projected [Ch.105 (1)]. The pterygoid fossa is shallow but clearly present, because the posterior edge of the pterygoid has two well-differentiated medial and lateral borders. The fossa extends above the roof of the internal nares [Ch.102 (1)], unlike in protosirenids (Domning & Gingerich, 1994; Bajpai *et al.*, 2009; Domning *et al.*, 2017). In the medial corner of the posteroventral extremity of the pterygoid process, there is a small posteromedial projection of the bone, which is here interpreted as the hamular trochlea, where the tensor veli palatini muscle or the pterygopharyngeus muscle is attached (Domning, 1977a; Domning & Gingerich, 1994). The pterygoids contact the palatines anteriorly, the basisphenoid dorsally and the alisphenoid laterally, although the sutures of the latter two are not clearly discernible.

Palatine: The palatines (Fig. 2: pal) and their contacts are well preserved in the paratype skull MPZ 2017/2, except for their posterior edges. The palatines are thin, flat bones that contact the maxillae anteriorly and laterally. Their anterior width is 23 mm. The two palatines are joined by a median suture from their anterior border, which extends at least as far as the midpart of P^5, and thus beyond the posterior edge of the zygomatic–orbital bridge [Ch.99 (0)], as in 'prorastomids', protosirenids and some other pan-sirenians, such as *Eotheroides* spp. and *Prototherium ausetanum* (Samonds *et al.*, 2009; Zalmout & Gingerich, 2012; Balaguer & Alba, 2016). The posterior border of the palatines is broken, and its morphology and limits are not clear, but it lies at least behind the anterior border of M^3 [Ch.97 (0,1)]. The remnant bone can be seen to be < 1 cm thick at the level of the penultimate cheek tooth [Ch.16 (0)]. There is no sign of the two foramina that mark the maxillopalatine suture in other sirenians. The expected posterior contact with the pterygoid is broken in the paratype skull, but it is preserved in the holotype skull and forms the anterior part of the pterygoid process.

Maxilla: The maxillae are well preserved laterally in the holotype skull *MPZ 2017/1*, but their ventral surface is better preserved in the paratype skull MPZ 2017/2, although the maxillae are fractured and compressed in this specimen (Fig. 1B: mx). The maxillae form a lyre-shaped palate. The medial contact between them is marked by a low keel that extends almost the total length of the bone in ventral view. The deflection of the maxilla begins at the level of the P^4 alveolus in *MPZ 2017/1*. The dorsoventral compression of MPZ 2017/2 disguises the rostral deflection of this specimen. The maxilla encloses a small infraorbital foramen (Fig. 1: fio) in the holotype skull [height, 16 mm; width, 8.3 mm; Ch.13 (0)], as in 'prorastomids', protosirenids and *Eotheroides aegyptiacum* (Abel, 1913; Domning & Gingerich, 1994; Savage *et al.*, 1994; Bajpai *et al.*, 2009). The infraorbital foramen is directed anteroventrally and is unobstructed [Ch.20 (0)]. Its outline is oval, but it is affected by the lateromedial compression of the skull. The infraorbital canal is short (13 mm in length) and extends from the anterior end of P^2 to the anterior end of P^4. The infraorbital foramina are placed 56 mm away from each other across the rostrum in the holotype skull and 51 mm in the paratype skull. The zygomatic–orbital bridges of the maxillae, which surround the infraorbital foramina, are long anteroposteriorly [60–65 mm in length; Ch.14 (0)]. Their anterior edges are thin and sharp, and the posterior ones are thicker and rounded [Ch.22 (0)]. The height of the zygomatic–orbital bridge above the alveolar shelf of M^1 is 20 mm, meaning that it is elevated above the palate [Ch.11 (1)], as in 'prorastomids' (Savage *et al.*, 1994) and the protosirenid *Ashokia* (Bajpai *et al.*, 2009). Anteriorly, the maxillae form a narrow palatal gutter [Ch.23 (0)] following the palate midline, unlike in protosirenids (Domning & Gingerich, 1994; Domning *et al.*, 2017), with tall but thin edges bordering the tooth roots in *MPZ 2017/1*. The maxillary dental arcade is concave medially, and the palate is narrowest at the level of P^1, from where it broadens and attains its maximum breadth across the anterior edge of M^1 in MPZ 2017/2 (44 mm).

The maxillary dental alveoli are evident. A single canine alveolus is situated immediately behind the premaxillary–maxillary suture [Ch.144 (1)]. There is no diastema between the C^1 alveolus and the I^3 alveolus in *MPZ 2017/1* (Fig. 2C). There is a small gap of 10 mm in MPZ 2017/2, but in this skull the ventral side of the maxilla is not preserved, meaning that this distance probably represents the spacing between the roots of the teeth and not a diastema between their crowns (Fig. 2A, B). Posterior to the canine alveolus, there are five alveoli for single-rooted P^1–P^5 on the right side [Ch.145 (0); Ch.157 (1)]. In the left dental arcade of *MPZ 2017/1*, the permanent P^5 is preserved [Ch.146 (0)]. In this skull, the diastema between the canine and the P^1 alveolus is 14 mm and that between the P^1 and P^2 alveoli is 14 mm on the

left side and 22 mm on the right side. The molar teeth (M^1–M^3) are preserved on both sides in *MPZ 2017/1* and MPZ 2017/2 (Fig. 2A–C). The space posterior to the maxillary dental battery is 12 mm in *MPZ 2017/1*. The maxilla contacts the premaxilla anterodorsally, the palatines ventromedially, the jugal dorsolaterally and the lacrimal posteriorly.

Squamosal: The squamosals are preserved in *MPZ 2017/1* (the holotype), but broken and displaced (Fig. 1: sq; Supporting Information, Table S2). The zygomatic arches (Fig. 1: zps) are lateromedially compressed and shifted against the cranial roof. The paratype MPZ 2017/2 preserves the zygomatic processes of the squamosal and part of their cranial portion (Fig. 2A, B). The skull MPZ 2020/591 preserves the left zygomatic process but isolated from the skull. Specimen MPZ 2020/603 is an isolated right squamosal (Fig. 8A–E), judged to belong to a mature individual owing to its size, which preserves the zygomatic process and the cranial portion. It is undeformed and preserves the original morphology of the squamosal in posterior view, which is distorted in the skulls. In addition, a right juvenile squamosal that lacks the dorsal cranial portion (MPZ 2020/604) and a dorsal portion and the distal part of a left juvenile squamosal (MPZ 2020/605) are preserved. These specimens are assigned to juvenile individuals on account of their small size (Fig. 8F–K; Supporting Information, Table S2).

In the paratype skull MPZ 2017/2 (Fig. 1A, B), the squamosal bones are out of place, but their position is more similar to the original position than in the holotype skull. The zygomatic breadth of this skull is 150 mm. The dorsal end or cranial portion of the squamosal contacts the parietal and reaches the nuchal crest but not the temporal crests, because these are joined and thus situated in a more dorsal position on the skull roof [Ch.76 (1)]. However, in lateral view there is not a significant distance between the squamosal and the top of the cranial roof as occurs in protosirenids (Domning & Gingerich, 1994; Bajpai *et al.*, 2009; Domning *et al.*, 2017), and the condition observed in *Sobrarbesiren* is more like that of the rest of the pan-sirenians.

The suture line with the parietal is interdigitated. The zygomatic process is robust, tapered anteriorly, and triangular in cross-section [Ch.81 (0)]. The left zygomatic process of *MPZ 2017/1* is 109 mm long anteroposteriorly and 35 mm wide dorsoventrally, with its maximum height in the middle part of the bone. The concave medial side of the zygomatic process is inclined inward dorsally [Ch.84 (0)]. Its ventral side shows an inflexion from the middle of the bone to its anterior edge; this inflexion marks the contact with the jugal (Fig. 8G, J). This contact surface is narrow and slightly concave. The root of the zygomatic process of the squamosal is 46 mm long anteroposteriorly in *MPZ 2017/1*, 42 mm in the specimen MPZ 2017/2 and 21 mm in the juvenile squamosal MPZ 2020/604. The rear edge of the zygomatic process is broken and out of place in the type skulls, but a moderately inflected processus retroversus (posterior end of the zygomatic process) can be observed on the right side of the skull MPZ 2017/2 [Ch.77 (1)]. This processus is absent in 'prorastomids' and protosirenids except *Libysiren* (Savage *et al.*, 1994; Domning, 2001a; Domning *et al.*, 2017).

The external auditory meatus in *MPZ 2017/1* (Fig. 1: eam) is narrow, 6 mm in anteroposterior length, 18 mm in dorsoventral height and 6 mm (right)/7 mm (left) in width between the postglenoid process (Fig. 2: pgp) and the post-tympanic process. Thus, it is higher dorsoventrally than anteroposteriorly [Ch.82 (0)]. The post-tympanic process projects anteroventrally and is enlarged, unlike in protosirenids except *Ashokia* (Domning & Gingerich, 1994; Bajpai *et al.*, 2009; Domning *et al.*, 2017), and the facet for insertion of the sternomastoid muscle is present [Ch.73 (0)].

The sigmoidal ridge (Fig. 8C: sr) is present and prominent in posterior view [Ch.74 (1)]. It projects laterally (~15 mm) in the specimen MPZ 2020/603 (Fig. 8A–E). Its dorsal part is lost, but the ventral part extends to the ventral tip of the post-tympanic process. The temporal condyle (or tuberculum; Fig. 2: tco) is prominent. The mandibular fossa (Fig. 2: maf) is a shallow and narrow depression 10 mm in anteroposterior breadth in MPZ 2017/2, and the postglenoid process (Fig. 2: pgp) is low and elongated. All of them are transversely directed. The squamosal–alisphenoid suture is not clear in the type skulls *MPZ 2017/1* and MPZ 2017/2, but it is well marked in the ventral view of the partial left squamosal of the skull MPZ 2020/591 (Fig. 2D). It is interdigitated and is located at the level of the medial border of the temporal fossa (Fig. 2: tf). The contact surface of the squamosal with the alisphenoid is also preserved in the specimen MPZ 2020/604 (Fig. 8H, K). Posteroventrally, the post-tympanic process of the squamosal contacts the paraoccipital process of the exoccipital.

Juvenile squamosals: The general morphology of the isolated juvenile squamosals MPZ 2020/604 and MPZ 2020/605 is like that of the adult and subadult skulls, although structures such as the sigmoidal ridge, the temporal condyle and the postglenoid process are less prominent, and the mandibular fossa is almost undefined (Fig. 8F–K). The external auditory meatus measures 9 mm in anteroposterior length, 12 mm in dorsoventral height and 4 mm in width between the postglenoid and the post-tympanic process in the specimen MPZ 2020/604.

Jugal: The jugals are broken and distorted in all the skulls (Fig. 1; Supporting Information, Table S2).

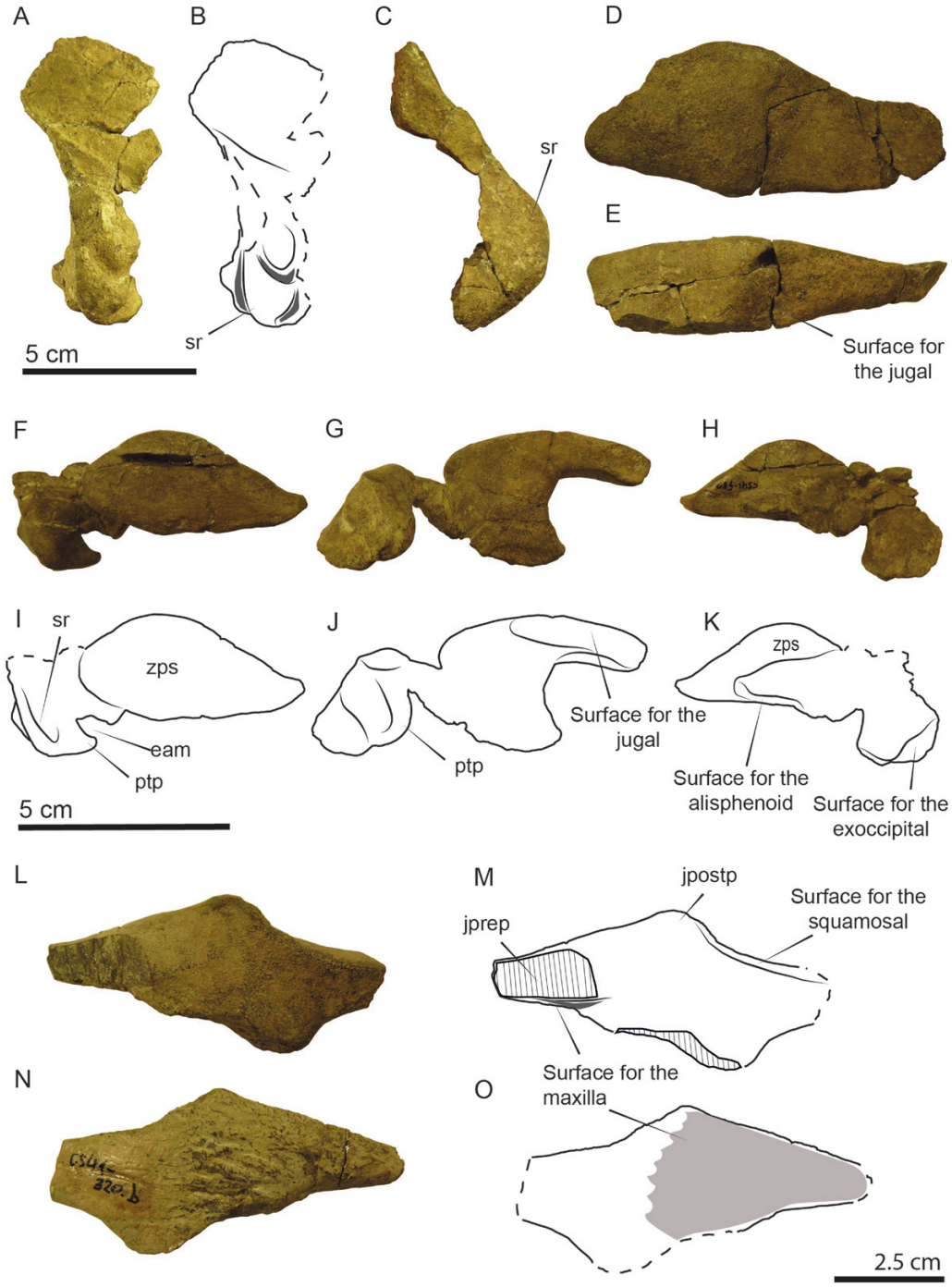

Figure 8. Isolated squamosals and jugal of *Sobrarbesiren cardieli*. A–E, MPZ 2020/603, right isolated squamosal; cranial portion in lateral view (A), interpretive sketch (B), and in posterior view (C); and zygomatic process in lateral (D) and ventral (E) views. F–K, MPZ 2020/604, right isolated juvenile squamosal in lateral (F), ventral (G) and medial (H) views, and interpretative sketches (I–K, respectively). L–O, MPZ 2020/606, left partial jugal in lateral (L) and medial (N) views, and interpretative sketches (M, O, respectively). Dashed lines indicate incomplete bones, and dashed areas denote broken surfaces. For abbreviations, see the Material and Methods section.

Specimen *MPZ 2017/1* preserves an almost complete left jugal, and MPZ 2017/2 has partly preserved jugals, which lack the ventral and postorbital processes. In addition, an isolated and incomplete left jugal (MPZ 2020/606) has been recovered (Fig. 8L–O). The jugal forms the ventrolateral margin of the orbit. The total

length of the left jugal of the holotype skull *MPZ 2017/1*, the most complete one, is estimated at 149 mm, with an approximate maximum dorsoventral height of 44 mm. In *MPZ 2017/1*, the preorbital process (Fig. 8: jpre) is a thin and short plate [Ch.88 (0)] that overlaps the maxilla but does not contact either the premaxilla or the lacrimal [Ch.87 (0)]. The jugal does not extend to the anterior margin of the orbit, which is formed by the lacrimal and the maxilla. The ventral process of the jugal is broken and shifted, and its shape is not clear. Its ventral border is rounded; the lateral surface is smooth, and it is lateromedially flattened. The position of this process with respect to the postorbital process is not clear in the type skulls. The postorbital process (Fig. 8: jpostp) is a rounded summit that lies against the zygomatic process of the squamosal. The zygomatic process of the jugal is long and narrow, and it thins towards its rounded end. This process is lateromedially flattened and longer than the anteroposterior diameter of the orbit [Ch.89 (0)]. It reaches the anterior edge of the temporal condyle. The isolated jugal MPZ 2020/606 has a total length of 70 mm and is 32 mm in height. It lacks the ventral and postorbital processess but preserves part of the preorbital process and part of the zygomatic process. The jugal is flattened lateromedially, with a maximum thickness of 11 mm. The ventral part of the preorbital process has a shallow step parallel to the process, where the maxilla contacts the jugal, the latter overlapping the former. The ventral rim of the orbit does not distinctly overhang the lateral surface of the jugal [Ch.90 (0)]. Although the ventral process of the jugal is not preserved, in accordance with the position of the fracture surface in this specimen, the ventral extremity of the jugal would be positioned posterior to the orbit or under the posterior edge of the orbit, but anterior to the postorbital process of the jugal [Ch.85 (0,1)].

Periotic: The right periotic is preserved, in part, in the paratype skull MPZ 2017/2 (Fig. 9A: pe), and only the pars petrosa can be described (Fig. 9A: pp). Only the ventral view can be observed because the bone is not isolated from the skull. In addition, an isolated right tegmen tympani (MPZ 2020/607) has been recovered (Fig. 9B, C). The periotic is situated in a socket formed by the squamosal and the exoccipital. Its anteroposterior length is 40 mm, and its estimated width is 43 mm. The pars petrosa is formed by swollen and dense bone. It is somewhat flattened dorsoventrally, and its posteromedial side is rounded. On its ventral surface, a blunt promontorium (Fig. 9: pm) and the perilymphatic foramen (Fig. 9: pf) are preserved. The endolymphatic foramen is not visible. The isolated tegmen tympani is elongated and is gradually tapered towards its pointed anteromedial end (Fig. 9B, C). It is not fused to the alisphenoid [Ch.115 (1)], as in all pan-sirenians except *Prorastomus* (Savage *et al.*, 1994). The anterior and ventral surfaces are rounded. The dorsal surface is also rounded but marked by a longitudinal groove. The posterior surface is covered by anteroposterior striations.

Tympanic: Three tympanic bones are recovered: the right and left tympanic of the holotype skull *MPZ 2017/1* and another isolated and incomplete tympanic associated with the skull MPZ 2020/591. The tympanic bone of *Sobrarbesiren* is swollen, horseshoe-shaped and asymmetrical, as is usual in sirenians (e.g. Robineau, 1969; Thewissen & Bajpai, 2009). The right tympanic of the holotype skull is the most complete recovered (Fig. 9D, E). Its anteroposterior length is 18 mm, and its dorsoventral height is 24 mm. Its anterior side is straight but shows a small anteromedially directed protuberance. The posterior side is straight in its dorsal half and inflected anteroventrally in its ventral half. The anterior and posterior sides join in a pointed apex, which is directed anteroventrally when situated in its original position in the skull. The anterior arm (Fig. 9: aa) is directed dorsomedially and is longer and more robust than the posterior one (Fig. 9: poa), which is directed dorsolaterally. The sulcus tympanicus is slightly marked at the base of the posterior arm. The lateral side of the tympanic bone is convex, and the medial side is concave and shows a shallow, elongated dorsomedial furrow. The tympanic arch (Fig. 9: ta; or lumen of the tympanic arch, following Voss & Hampe, 2017) has an internal diameter of 5 mm, which is relatively narrow compared with other sirenians. The tympanic bone of *Sobrarbesiren* is anteroposteriorly broad and more robust than the tympanic bone of *Prorastomus*, although the two taxa share a relatively narrow arch (Supporting Information, Table S3; Savage *et al.*, 1994). The tympanic bone of *Eotheroides lambondrano* is similar in size to that of *Sobrarbesiren*, but its internal diameter is twice as great (Fig. 10C; Supporting Information, Table S3). Other Eocene pan-sirenians also possess proportionally broader tympanic arches than *Sobrarbesiren*. These include *Protosiren smithae* (Domning & Gingerich, 1994: fig. 3), '*Halitherium*' *taulannense* (holotype skull *RGHP D040*), '*Prototherium*' *intermedium* (skull MGP-PD 28998) and *Eotheroides clavigerum* (Zalmout & Gingerich, 2012: fig. 29A). The condition of a tympanic bone with a broad tympanic arch is maintained in post-Eocene taxa, such as *Metaxytherium albifontanum* Vélez-Juarbe & Domning, 2014 (Fig. 10D; Supporting Information, Table S3) and extant sirenians (Robineau, 1969: figs 8, 10E).

Malleus, incus and stapes: Not preserved.

Mandible: Mandibles are represented by only a partial left ascending ramus (MPZ 2020/608), which preserves

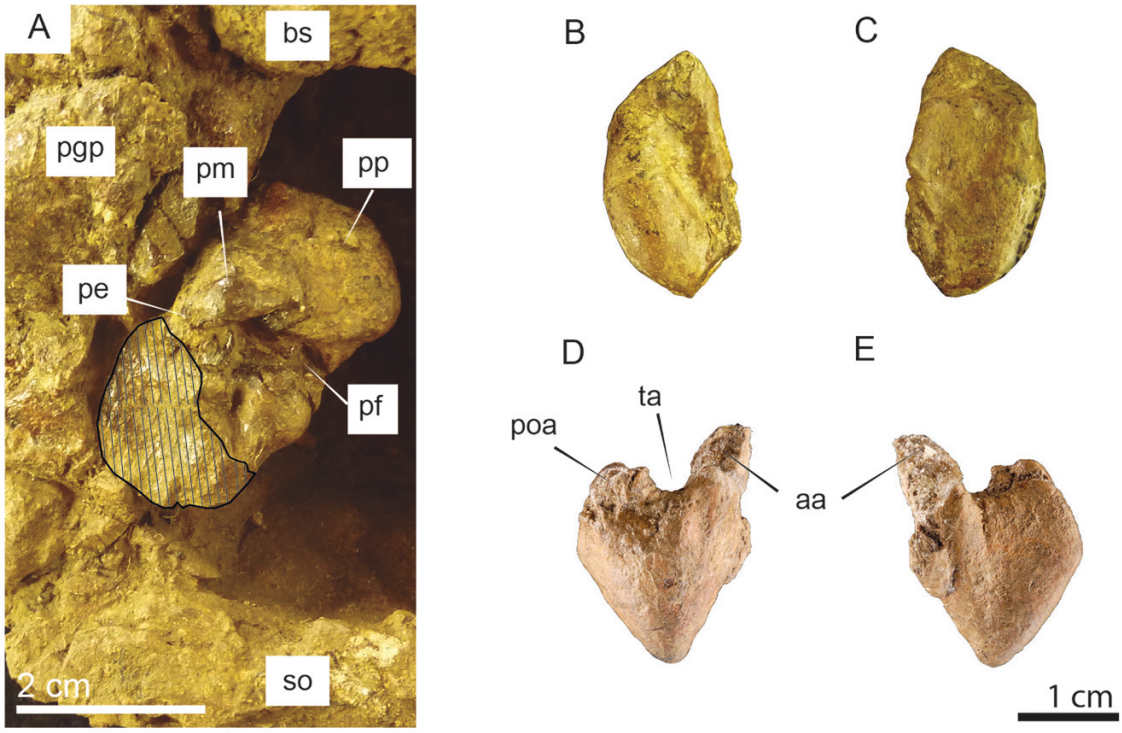

Figure 9. Bones of the ear region of *Sobrarbesiren cardieli*. A, right periotic of the paratype skull MPZ 2017/2 in ventral view. B, C, MPZ 2020/607, right pars temporalis (= tegmen tympani) in ventral (B) and dorsal (C) views. D, E, right tympanic of the holotype skull *MPZ 2017/1* in lateral (D) and medial (E) views. Dashed areas denote broken surfaces. For abbreviations, see the Material and Methods section.

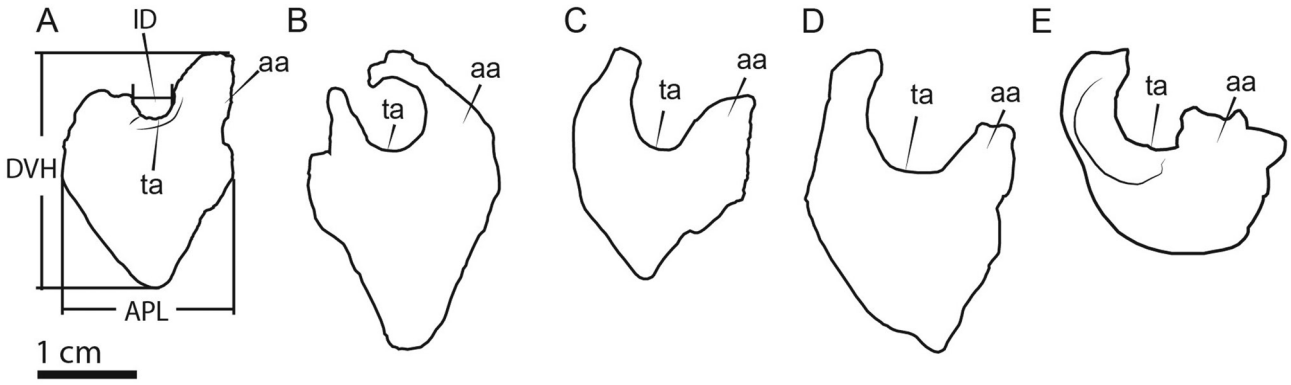

Figure 10. Schematic drawings of tympanic bones of various sirenian taxa. A, *Sobrarbesiren cardieli*, right tympanic of the holotype skull *MPZ 2017/1*. B, *Prorastomus sirenoides*, right tympanic *BMNH 44897*. C, *Eotheroides lambondrano*, left tympanic (from Samonds *et al.*, 2009: fig. 6B). D, *Metaxytherium albifontanum*, right tympanic (from Vélez-Juarbe & Domning, 2014: fig. 8A). E, *Trichechus senegalensis*, right tympanic (from Robineau, 1969: fig. 11, not to scale). For abbreviations, see the Material and Methods section. Measurements: APL, Anteroposterior length; DVH, Dorsoventral height; ID, Internal diameter.

the condyle (Fig. 11A, B: con) and part of the coronoid process (Fig. 11A, B: cp). This mandibular fragment is 47 mm in length and 50 mm in height, and its ventral and posterior borders are broken. The articular surface of the mandibular condyle is suboval in dorsal view, convex and inclined medially. Its lateral side is rounded, and the medial side is pointed and slightly narrower. It is 11 mm in anteroposterior length and 18 mm in lateromedial width. It is as extended medially as laterally, as in some Eocene pan-sirenians (Sagne, 2001a: Ch.53) and unlike the clearly extended and medially projected articular surface of *Prorastomus*

(Savage *et al.*, 1994: fig. 6), *Pezosiren* (holotype, *USNM 511925*) and *Protosiren smithae* (cast CGM 4229 of the holotype *94810*). The mandibular notch is preserved, and it is narrow. The coronoid process clearly rises above the level of the dorsal edge of the condyle, despite being broken. The preserved lamina of the coronoid process is thin, 4 mm in thickness. In medial view, there is an elongated groove below the condyle, oriented dorsoposteriorly to anteroventrally, which Domning (1977a) interprets as the insertion area for the pterygoideus externus muscle.

Dentition: The type skulls *MPZ 2017/1* and MPZ 2017/2 preserve the M^1–M^3 molar series on both sides and alveoli for incisors, canines and the P^1–P^5 premolar series, with the left P^5 being preserved in the holotype skull (Figs 1C, 2C). On the basis of the preserved alveoli and their position, the upper dental formula of *Sobrarbesiren* has been interpreted as 2.1.5.3 [Ch.139 (0); Ch.143 (0); Ch.145 (0); Ch.146 (0); Ch.150 (0); Ch.151 (0); Ch.155 (1)] (Díaz-Berenguer *et al.*, 2018). Therefore, *Sobrarbesiren* retains a single-rooted permanent P^5, like the 'prorastomid' *Pezosiren* and protosirenids (Abel, 1907; Domning & Gingerich, 1994; Domning, 2001b) and unlike the three-rooted permanent premolar of *Prorastomus* (Savage *et al.*, 1994). However, it shows a reduction in the number of incisors by the loss of I^2, like *Prototherium* spp. and the *Eotheroides* spp. from Egypt, although the condition for *Eotheroides aegyptiacum* is unknown (Bizzotto, 1983; Pilleri *et al.*, 1989; Zalmout & Gingerich, 2012).

In addition, two isolated incisors were tentatively identified as an $?I^1$ (MPZ 2017/4) and an $?I^3$ (MPZ 2017/5) (Fig. 12A–D). The description of the incisors, the P^5 and the molar series was included in the paper by Díaz-Berenguer *et al.* (2018). The alveoli of the canines and premolars in both skulls indicate that these teeth were single rooted [Ch.144 (1); Ch.157 (1); Fig. 2]. Subsequently, several isolated premolars have been recovered. Preliminarily, they are considered upper premolars on the basis of the scarcity of mandibles in the CS-41 fossil site. Specimen MPZ 2020/610 (Fig. 12E–G) is identified as a right upper premolar ($?P^2$) and MPZ

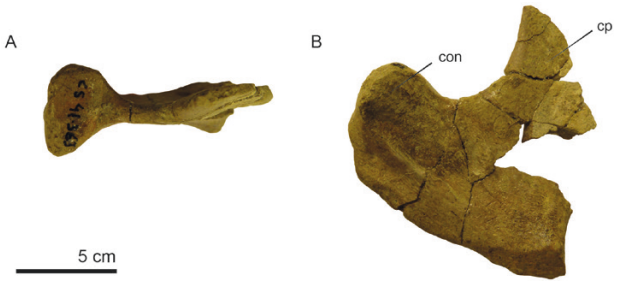

Figure 11. Mandibular fragment of *Sobrarbesiren cardieli* (MPZ 2020/608) in dorsal (A) and medial (B) views. For abbreviations, see the Material and Methods section.

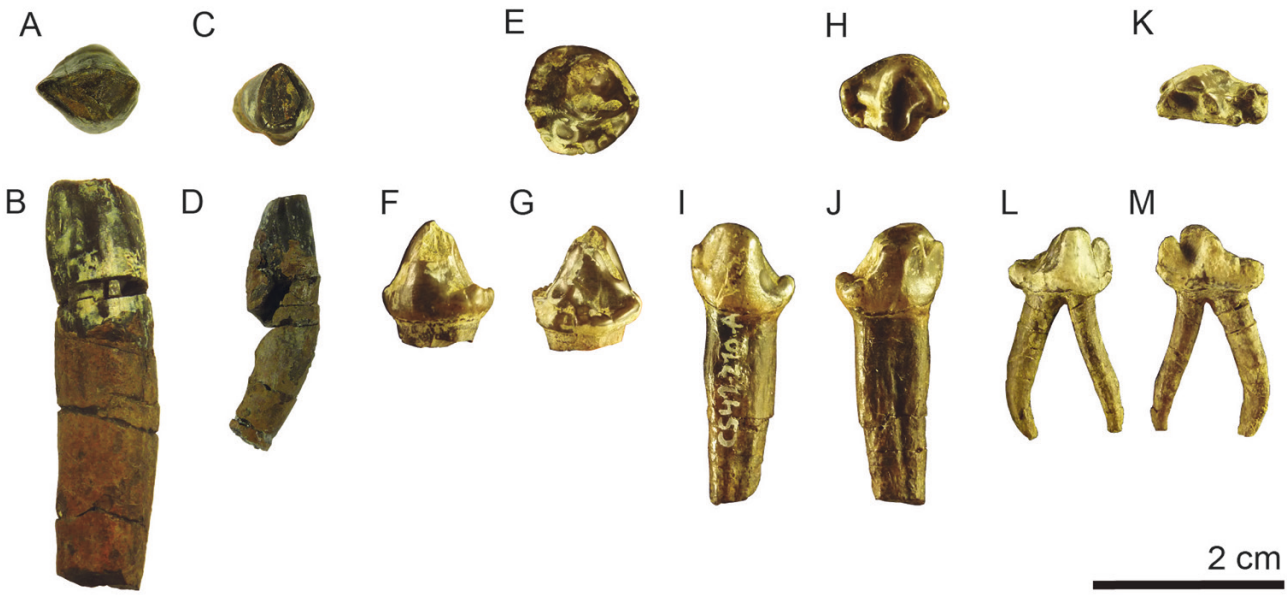

Figure 12. Isolated teeth of *Sobrarbesiren cardieli*. A, B, $?I^1$ (MPZ 2017/4) in occlusal (A) and labial (B) views. C, D, $?I^3$ (MPZ 2017/5) in occlusal (C) and lateral (D) views. E–G, P^2 (MPZ 2020/610) in occlusal (E), labial (F) and lingual (G) views. H–J, $?P^{3–4}$ (MPZ 2020/611) in occlusal (H), labial (I) and lingual (J) views. K–M, deciduous premolar (MPZ 2020/614) in occlusal (K), labial (L) and lingual (M) views.

2020/611–612 as left ?P^{3-4} (Fig. 12H–J). Specimen MPZ 2020/613 is an undetermined worn upper premolar, and MPZ 2020/614 (Fig. 12K–M) is a deciduous premolar (left ?DP^3). For the dental measurements, see the Supporting Information (Table S4).

Specimen MPZ 2020/610 is considered a ?P^2 because it shows only one contact with an adjacent tooth, in this case probably P^3. The crown is composed of a main central cusp, partly worn and exposing the dentine, and a posterolingual low accessory cusp. A cingulum with numerous cuspules covers the anterior, lingual and posterior perimeter of the tooth. The root is absent.

Specimens MPZ 2020/611–612 are considered ?P^{3-4} because their crowns possess two contact surfaces with adjacent teeth, and their morphology is different from that of the P^5 of the holotype skull (Fig. 2C). The crown is worn, but it preserves a main central cusp located labially and a lower secondary cusp located lingually. There is a strong and short anterolingual cingulum with three small cuspules. The main cusp and the cingulum are connected by two parallel cristae, and posterior to the main cusp there is another crista.

Specimen MPZ 2020/613 is a worn uniradiculate premolar and is partly broken. The main cusp has almost disappeared owing to wear, but this premolar possesses a cingulum with cusplets and an accessory cusp.

Specimen MPZ 2020/614 is a biradiculate deciduous premolar. It is preliminarily interpreted as a left DP^3 based on the number of roots for the deciduous premolars proposed for other fossil sirenians, such as *Prototherium veronense*, '*Halitherium*' *taulannense* and *Dusisiren* spp. (Sickenberg, 1934; Domning, 1978; Sagne, 2001a). This interpretation is also supported by the lack of contact surfaces with other premolars, which is in accordance with the sequence of dental eruption proposed by Sagne (2001a) for the Eocene pan-sirenian '*Halitherium*' *taulannense*. The crown of the tooth has a main labial cusp and two slightly lower anterior and posterior cusps. There is also a small lingual cusp. A small cingulum with one accessory cusp is located anteriorly. A strong posterior cingulum, labiolingually narrower than the rest of the crown and almost quadrangular in shape, is divided into three accessory cusps. Anterior and posterior roots are complete, separated and divergent.

Phylogenetic analysis

The phylogenetic analysis is based on an updated version of the matrix of Vélez-Juarbe & Wood (2018). Several modifications are made to the original dataset. The scores of *Sobrarbesiren* are updated with the new material and descriptions. In total, this new version of the dataset includes 62 taxa comprising an ingroup of 60 pan-sirenians plus the proboscidean *Phosphatherium escuilliei* Gheerbrant *et al.*, 1996 and the desmostylian *Cornwallius sookensis* Cornwall, 1922, which are used as the outgroups.

Codification of neurocranial bones

Six new characters are added to the dataset to address the anatomical observations on the morphology of the endocranial surface and basioccipital bone discussed above. The six characters are as follows:

Character 223. Ossified falx cerebri on the endocranial surface of the parietal (Sagne (2001a: Ch.23): (0) present and prominent; (1) absent.

The existence of the bony falx cerebri can be inferred in fossil sirenian taxa by the existence of a median sulcus on the dorsal surface of brain endocasts (Edinger, 1933) or by an ossified sagittal crest along the midline of the ventral surface of the parietals (Fig. 13A: bf). In taxa where the bony falx cerebri is absent, there is a shallow sulcus separating the two parietals (Fig. 13B: fce; e.g. *Sobrarbesiren*, *Protosiren fraasi* and *Libysiren sickenbergi*, Gingerich *et al.*, 1994; Domning *et al.*, 2017). In the prorastomid *Pezosiren* neither this sulcus nor a sagittal crest is present, but there is a tiny ridge (USNM 353586). This condition is also scored as a '0' by the authors.

When the falx cerebri is present, it can be sharp or low, reaching the frontoparietal suture [e.g. *Metaxytherium subapenninum* Sorbi *et al.*, 2012; *Metaxytherium arctodites* Aranda-Manteca *et al.*, 1994; '*Halitherium*' *taulannense* (specimen RGHP D057); *Nanosiren sanchezi* Domning & Aguilera, 2008], or its anterior end can be flattened and/or marked by a median

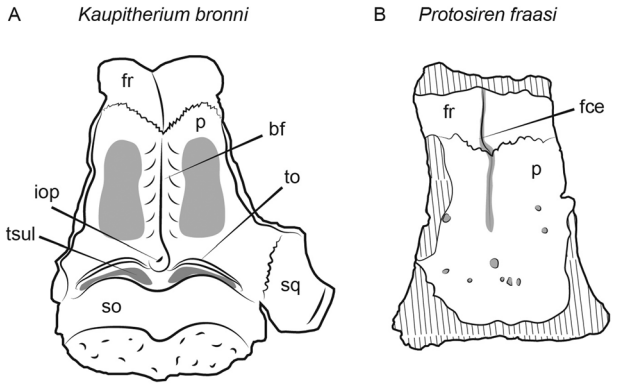

Figure 13. Endocranial surfaces of two sirenian skulls. A, *Kaupitherium bronni* (sketch based on Voss & Hampe, 2017: figs 4, 11). B, *Protosiren fraasi* (sketch based on Sickenberg, 1934: plate I, fig. 4). For abbreviations, see the Material and Methods section.

sulcus (e.g. *Metaxytherium albifontanum*, Vélez-Juarbe & Domning, 2014; *Dioplotherium manigaulti* Cope, 1883, Domning, 1989). Nevertheless, all these differences in the development of the bony falx cerebri can be found as intraspecific variations when studying numerous specimens of one taxon (e.g. *Metaxytherium floridanum* Hay, 1922, Domning, 1988), and for this reason all of them are scored as a '0' by the authors.

Character 224. Tentorium osseum on the endocranial surface of the parietal (new): (0) absent; (1) present.

According to Gingerich *et al.* (1994: 47), the tentorium osseum can be observed on the dorsal surface of brain endocasts as 'a distinct transverse groove passing through the deep median pit for the internal occipital protuberance'. In skulls, the tentorium osseum can be observed in the ventral view of the skull roof, as a transverse ridge in the line of fusion of the parietal and supraoccipital on both sides of the internal occipital protuberance (Fig. 13: to).

Some intraspecific variability in the presence–absence of the tentorium osseum has been observed in the stem pan-sirenians *Protosiren fraasi* and *Protosiren smithae*, some specimens of which lack the tentorium osseum, whereas others possess a low one (Domning & Gingerich, 1994; Gingerich *et al.*, 1994). In these cases, the character is scored as (0,1).

Character 225. Internal occipital protuberance on posterior ventral side of the parietal (new): (0) absent; (1) present.

The internal occipital protuberance appears in the posterior part of the parietals in ventral view, and it is the point where the bony falx cerebri and the tentorium osseum meet. According to our observations on *Sobrarbesiren*, the internal occipital protuberance can be present even though the bony falx cerebri is absent.

The internal occipital protuberance can be a low bump (*Dioplotherium manigaulti*, Domning, 1989; *Rytiodus heali* Domning & Sorbi, 2011) or it can be a sharply pointed protuberance (*Kaupitherium gruelli*, Voss & Hampe, 2017; *Metaxytherium arctodites*, Aranda-Manteca *et al.*, 1994). However, these slightly different morphologies might be attributable to intraspecific variation (Domning, 1988).

Character 226. Morphology of the basioccipital in ventral view (new): (0) trapezoidal, with the anterior end narrower than the posterior end; (1) rectangular, same width along its length; (2) hourglass-shaped, waisted at its midpart.

The morphology of the basioccipital bone in ventral view varies from the anterior end being narrower than the posterior one, as is the case in the 'prorastomids' (Fig. 14A), to an hourglass-shaped basioccipital with a characteristic waisted midpart (Fig. 14C–E). State (1) is considered an autapomorphy of *Sobrarbesiren*, in which the basioccipital lacks a waisted midpart and preserves the same width along its length (Fig. 14B).

Character 227. Insertions for the longus capitis muscle on the ventral side of the basioccipital (redefined from Sagne, 2001a: Ch.37): (0) shallow fossae; (1) deep fossae; (2) rugose protuberances or convexities.

The longus capitis muscle, involved in the flexion of the head, inserts onto the occipitosphenoidal eminence (or tuberculum pharyngeum, Kaiser, 1974) of the skull in extant sirenians, a paired convex rugose area on the anterior part of the ventral side of the basioccipital (Domning, 1977a). Nevertheless, in some fossil sirenians this insertion area is not an eminence but a paired concavity. Sagne (2001a) proposed Ch.37: 'Insertions des muscles nuchaux sur la face ventral du basioccipital' and differentiated two character states: deep fossae and rugose convexities. The phylogenetic character proposed here is redefined from that of Sagne (2001a) with the addition of a third character state to differentiate between shallow and deep fossae. It is considered that a taxon shows shallow fossae when these are shallow depressions that lack well-marked borders (state 0 of *Prorastomus* and *Sobrarbesiren*; Fig. 14A, B), unlike the fossae considered deep, which may vary between depressions with well-marked borders (state 1 in *Eotheroides aegyptiacum*; Fig. 14C) and those with deep concavities (state 1 in '*Halitherium*' *taulannense*; Fig. 14D). Protosirenids and dugongids possess rugose convexities (state 2 in *Protosiren fraasi*; Fig. 14E).

Character 228. Basioccipital mid-ventral keel (new): (0) present, reaching the posterior part of the basioccipital or extending beyond the posterior end of the insertion areas of the longus capitis muscle; (1) absent.

The presence of a thin keel on the ventral side of the basioccipital has been observed in some basal sirenians (e.g. *Prorastomus*, *Sobrarbesiren* and *Eotheroides aegyptiacum*; Fig. 14A–C); this extends from the anterior border of the basioccipital and beyond the posterior end of the insertion areas of the longus capitis muscle (state 0). Taxa that possess deep fossae may show a basioccipital keel, but this is a partition between these concavities, and for this reason it does not extend beyond the posterior edge of the fossae (state 1 in '*Halitherium*' *taulannense*; Fig. 14D).

Analysis settings

With the incorporation of these six new characters, the resulting dataset comprises 89 parsimony-informative characters. All characters were equally weighted a priori, and multistate characters were treated as unordered, as in the original analysis. Following the results of Springer *et al.* (2015), which

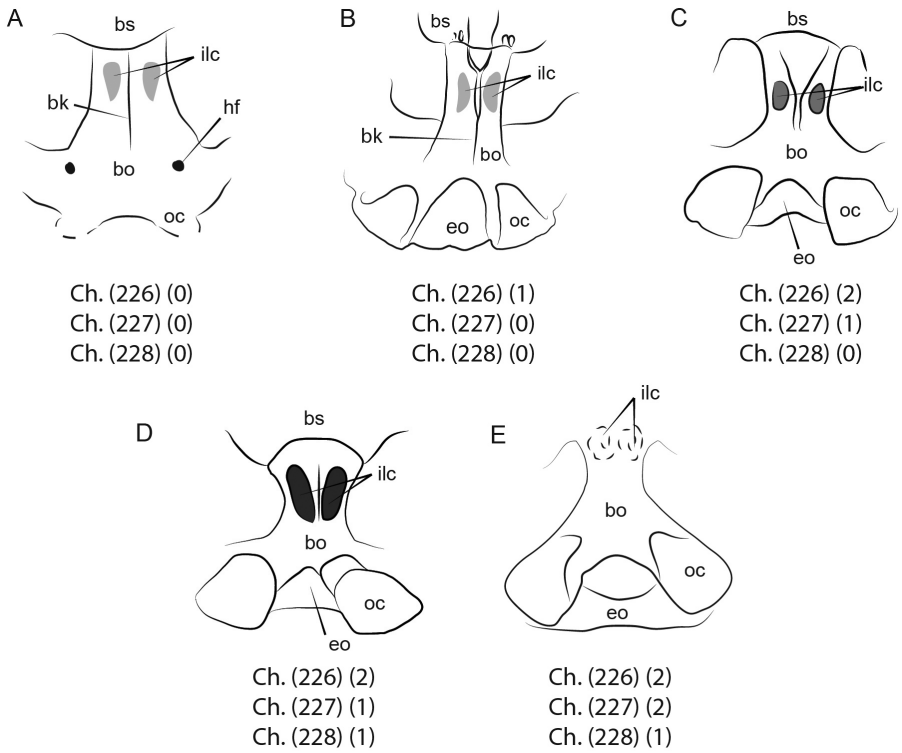

Figure 14. Comparison of basicranial region of various Eocene sirenian skulls. A, *Prorastomus sirenoides* (sketch based on holotype *BMNH 44897*). B, *Sobrarbesiren cardieli* (*MPZ 2017/1*). C, *Eotheroides aegyptiacum* (sketch based on Abel, 1913: table (II) XXXI, fig. 2). D, '*Halitherium*' *taulannense* (sketch based on holotype *RGHP D040*). E, *Protosiren fraasi* (sketch based on the BMNH skull cast PV M 9367). For abbreviations, see the Material and Methods section.

recovered a closer relationship between the genera *Hydrodamalis* and *Dugong* than with *Trichechus*, a backbone constraint was used to disregard trees with topologies not showing this relationship, as was proposed by Vélez-Juarbe & Wood (2018). Two parsimony-based analyses were applied to this dataset. A first analysis used a heuristic search with 1000 Wagner trees as starting trees, followed by tree bisection–reconnection (TBR), retaining ten most parsimonious trees (MPTs) per replication, followed by an additional round of TBR using all recovered trees. Owing to the lack of resolution of the first analysis, a second analysis was conducted, using implied weighting (Goloboff, 2014). Owing to the high number of missing entries in the dataset (a recurring problem in fossil datasets), the extended version of the implied algorithm was preferred. Missing entries were assumed to have 50.0% of the homoplasy of observed entries; homoplasy in missing entries was not increased beyond four times the observed homoplasy. A concavity constant of $k = 12$ was used to weight homoplasic characters.

Branch support was calculated using Bremer indices for the equal weights analysis and bootstrap values after 1000 replicates for both analyses.

RESULTS

Velez-Juarbe & Wood (2018) presented the most inclusive sirenian analysis to date, with good resolution for the crown clade Sirenia but showing a large polytomy for all stem pan-sirenians other than *Prorastomus*, the basalmost sirenian. Thus, the relationships among the pan-sirenians remain unresolved for the first 14 Myr of evolution of this clade.

The six new characters added in our analysis help to shed light on these relationships. In our equal weights analysis, the general topology of the consensus tree (Fig. 15A; Supporting Information, Fig. S1) of the 7560 MPTs (length = 310 steps; consistency index = 0.442; retention index = 0.777; rescaled consistency index = 0.344) is identical to that of Velez-Juarbe & Wood (2018), with a well-resolved crown clade Sirenia, but the relationships between the stem forms are more resolved. As in previous studies (Sagne, 2001a; Domning *et al.*, 2017; Díaz-Berenguer *et al.*, 2018), a clade containing *Libysiren*, *Protosiren* and *Ashokia*, namely Protosirenidae, is recovered, although in a more derived position than in former phylogenies and excluding Trichechidae (*contra* Sagne, 2001a; Domning *et al.*, 2017). Successive nesting clades show

the relationships of other stem forms: the *Eosiren* species are recovered in a polytomy with the clade that includes both *Eotheroides* species described by Zalmout & Gingerich (2012), which is sister to the clade comprising Sirenia and a smaller clade including '*Halitherium*' *taulanense* and the '*Prototherium*' *intermedium* wastebasket taxon (Domning, 1996). This clade was previously recovered in other phylogenetic proposals, but in a different position (Balaguer & Alba, 2016; Díaz-Berenguer *et al.*, 2018).

The root of the tree is not resolved completely. After the successively nesting 'prorastomids', a polytomy of stem forms is recovered, including *Sobrarbesiren*, *Eotheroides aegyptiacum*, *Prototherium ausetanum* and *Prototherium veronense*, with *Eotheroides lambondrano* slightly more deeply nested in a polytomy with Protosirenidae and all other pan-sirenians.

To explore the relationships in the stem group further, a second analysis was conducted, using extended implied weights with a soft concavity constant (k = 12). This analysis downweights the more homoplasic characters, favouring those characters that vary less along the MPTs, thus being more homological and less susceptible to convergences and reversions. The topology of the consensus (Fig. 15B; Supporting Information, Fig. S2) of the 945 MPTs recovered (fit = 10.75914; consistency index = 0.442; retention index = 0.777; rescaled consistency index = 0.344) is compatible with the equal weights consensus, but the relationships of the stem taxa are completely resolved. Protosirenidae is recovered as sister to the most inclusive clade composed of *Eotheroides lambondrano*, *Dugong dugon* and *Trichechus manatus*, and this clade is sister to a newly identified clade. This new clade can be defined as the smallest clade containing *Sobrarbesiren cardieli* but not *Dugong dugon*; it includes the internal specifier *Sobrarbesiren cardieli* plus the taxa *Eotheroides aegyptiacum*, *Prototherium veronense* and *Prototherium ausetanum*. Most interestingly, *Sobrarbesiren cardieli* is recovered as the basalmost form of the clade.

It is important to note that the general support for the tree is relatively low, with no basal clades showing Bremer indices higher than two and bootstrap values > 70, as in most phylogenies concerning the pan-sirenians (Fig. 15). These recovered topologies, despite being informative, will thus be subject to change as studies of new taxa and much-needed revisions of some basal taxa are included in the analysis.

DISCUSSION

Sobrarbesiren is a basal quadrupedal taxon that possesses an alisphenoid canal, a permanent P^5, a small infraorbital foramen and a narrow meatus auditorius, all of which are considered primitive conditions for sirenians, combined with derived characteristics such as a deflected rostrum, albeit in a low degree, a shortened sphenopalatine region, the presence of the processus retroversus and the loss of the upper second incisor.

In the various phylogenetic proposals published previously, *Sobrarbesiren* is recovered as the sister taxon of a paraphyletic group then defined as 'Dugongidae' (the clade that includes all pan-sirenians except the 'prorastomids' *Prorastomus* and *Pezosiren*; the protosirenids and *Sobrarbesiren*; Díaz-Berenguer *et al.*, 2018) or it is included in a polytomy with the rest of the Eocene sirenians except *Prorastomus* (Vélez-Juarbe & Wood, 2018). In our phylogenetic proposal, *Sobrarbesiren* forms a clade with *Eotheroides aegyptiacum*, *Prototherium veronense* and *Prototherium ausetanum*. This is the sister clade of the rest of the pan-sirenians except the 'prorastomids'; hence, the position of *Sobrarbesiren* as a basal stem pan-sirenian is maintained independently of the different phylogenetic proposals.

The new topology of the recovered tree shows the importance of including neurocranial characters in the phylogeny of Pan-Sirenia. The six new characters added (Ch.223–228) not only increase the resolution of the consensus topology, but also provide further support for previously established clades (Fig. 16; Supporting Information, Figs S3–S8). For example, character 227 (insertions for the longus capitis muscle on the ventral side of the basioccipital) supports the monophyly of Protosirenidae established in previous phylogenetic proposals (e.g. Velez-Juarbe *et al.*, 2012; Vélez-Juarbe & Domning, 2014; Díaz-Berenguer *et al.*, 2018). The new clade formed by *Sobrarbesiren*, *Prototherium veronense*, *Prototherium ausetanum* and *Eotheroides aegyptiacum* is supported by character 225: 0→1 (Fig. 16; Supporting Information, Fig. S5), with *Sobrarbesiren cardieli* being well differentiated from more derived forms by one local autapomorphy, 227: 1→0, and another autapomorphy, 226: 2→1 (Fig. 16; Supporting Information, Figs S6, S7).

We refrain from naming the newly recovered clade that includes *Sobrarbesiren cardieli* mainly on account of the low general support obtained for the topologies. We believe that it is worth further exploration of its position and relationship to other stem forms rather than naming a possibly unstable clade. In addition, Protosirenidae is recovered as a more derived clade than these stem forms, contrary to all previous analyses, where Protosirenidae is recovered as the basalmost clade after the 'prorastomids' (e.g. Vélez-Juarbe & Domning, 2014; Springer *et al.*, 2015; Balaguer & Alba, 2016; Domning *et al.*, 2017; Díaz-Berenguer *et al.*, 2018). Again, this position must be taken with caution because of the low support of the

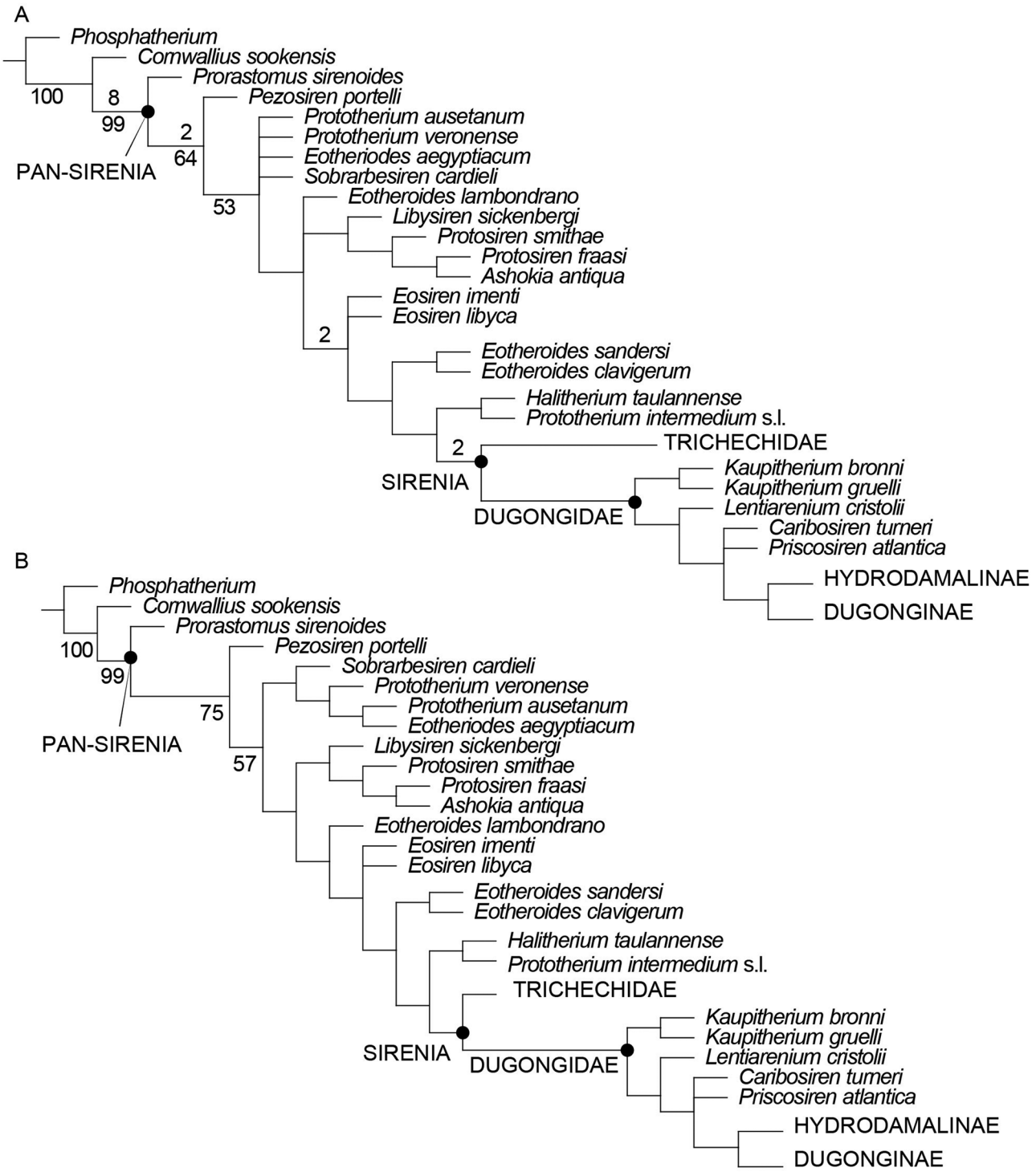

Figure 15. Phylogenetic relationships of Pan-Sirenia, after updating and reanalysing the dataset of Velez-Juarbe & Wood (2018). A, consensus tree of the 7560 most parsimonious trees (MPTs) with equally weighted characters (length = 310 steps; consistency index = 0.442; retention index = 0.777; rescaled consistency index = 0.344). B, consensus tree of the 945 MPTs under implied weighting analysis (concavity constant, k = 12; fit = 10.75914; consistency index = 0.442; retention index = 0.777; rescaled consistency index = 0.344). Numbers above branches represent the Bremer index, with values below two not represented. Numbers below branches represent bootstrap values > 50, after 1000 replications. Clade names and definitions follow Velez-Juarbe & Wood (2018).

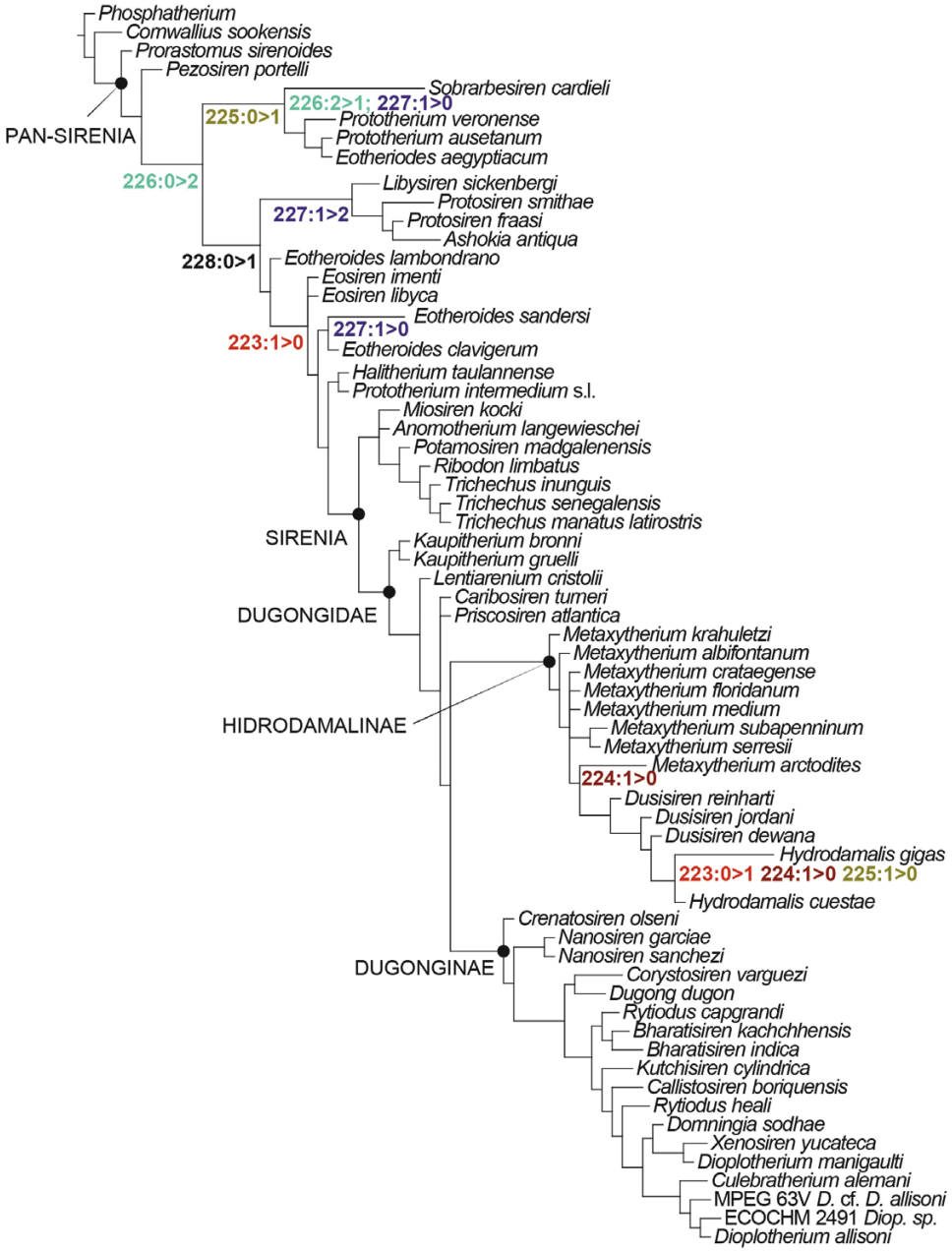

Figure 16. Synapomorphies common to all the most parsimonious trees mapped on the implied weighting consensus topology. The six new characters (223-228) described in the present study are mapped. See main text for descriptions of characters and states.

topology. Further research is needed to evaluate this topology.

As mentioned above, it is interesting to note that the species of *Prototherium* do not form a clade, supporting the idea that '*Prototherium*' *intermedium* probably pertains to a different genus, as proposed by Domning (1996), and furthermore, to a more derived clade, as recovered in other cladistic analyses (e.g. Balaguer & Alba, 2016; Díaz-Berenguer *et al.*, 2018).

Furthermore, the topology of the recovered phylogenetic tree highlights interesting questions with respect to the endocranial structures (Ch.223–225). The absence of the falx cerebri, tentorium osseum and internal occipital protuberance has traditionally been considered diagnostic of protosirenids (Sickenberg, 1934; Domning & Gingerich, 1994). Nevertheless, after analysing the rudimentary endocranial structures in *Pezosiren*, Domning *et al.* (2017) propose that their

absence could be a primitive condition in dugongids and trichechids. The reconstruction of Ch.223–225 (Supporting Information, Figs S3–S5) supports the hypothesis that the absence of endocranial structures is the plesiomorphic condition for pan-sirenians, hence not diagnostic for Protosirenidae. This assumption implies that the assignment of certain fragmentary European specimens to Protosirenidae must be reconsidered (Delfortrie, 1872; *sensu* Sickenberg, 1934).

Sobrarbesiren lacks a bony falx cerebri but possesses a tentorium osseum and internal occipital protuberance, evidencing that the development of these structures is not synchronic. The presence of the tentorium osseum and the internal occipital protuberance in the perinatal specimens of *Sobrarbesiren* (MPZ 2020/598 and MPZ 2020/599) suggests that they ossified before birth in the fossil sirenians, as happens in extant *Dugong dugon* (Nojima, 1988). Phylogenetically, the ossification of the falx cerebri in sirenians appears for the first time during the Lutetian (middle Eocene), with the Egyptian taxon *Eotheroides aegyptiacum*.

With respect to the phylogenetic characters based on the basioccipital bone, [morphology of the basioccipital bone in ventral view (Ch.226) and basioccipital mid-ventral keel (Ch.228)], these have a clear phylogenetic signal (Supporting Information, Figs S6, S8). These characters reveal that the presence of a low ventral keel along the midline of the basioccipital, as in 'prorastomids', *Eotheroides aegyptiacum* and *Sobrarbesiren*, could be considered the plesiomorphic condition for sirenians and that the morphology of the basioccipital has varied during the evolution of sirenians. The character 'insertions for the longus capitis muscle on the ventral side of the basioccipital' (Ch.227) is highly homoplasic, but useful for grouping the clade Protosirenidae and Dugongidae (Supporting Information, Fig. S7). Thus, the basioccipital bone is a key structure with strong phylogenetic implications that should be studied in detail and coded adequately in future studies.

Intraspecific cranial variations in *Sobrarbesiren cardieli*

The studied specimens of *Sobrarbesiren cardieli* represent at least eight different individuals based on complete and partly complete skulls and isolated cranial bones at different ontogenetic stages from perinatal to young adult individuals. Nevertheless, the perinatal and juvenile individuals are represented by isolated skull bones that do not allow patterns of cranial development to be inferred. Hence, sound inferences regarding the ontogenetic development of *Sobrarbesiren* are precluded, although some observations can be made. The specimens do not show strong intraspecific variation, but some differences come to light when the studied material is compared.

Intraspecific variations in the morphology or grade of development of the temporal crests have been described in various sirenian taxa, such as '*Halitherium*' *taulannense*, *Kaupitherium gruelli* and *Metaxytherium floridanum*. These have been associated with the ontogenetic development of the individuals (Domning, 1988; Sagne, 2001a; Voss & Hampe, 2017). The three complete to partly complete skulls of *Sobrarbesiren* (*MPZ 2017/1*, MPZ 2017/2 and MPZ 2020/591) show differences in the development of the temporal crests. The crests are joined in the specimens *MPZ 2017/1* and MPZ 2020/591, whereas they are slightly separated in MPZ 2017/2 (Fig. 4). This feature could support the hypothesis that the paratype skull represents a slightly younger individual than *MPZ 2017/1* and MPZ 2020/591. With respect to the juvenile individuals, the skullcap MPZ 2020/598 has incipient and separated temporal crests (Fig. 6C, D). However, they cannot be identified in the skullcap MPZ 2020/599, probably owing to the preservation of this fossil.

Furthermore, Sagne (2001a) highlights the differential development of the temporal crests during growth in the dorsal surface of frontals and parietals in '*Halitherium*' *taulannense* and proposes the following variations: the temporal crests are thin and prominent on the frontal and absent on the parietal in the skull of a newborn, absent on the frontal and thin on the parietal in older but still young specimens, and they are marked on both the frontal and the parietal in older subadult and adult skulls. In the skulls assigned to subadult–adult individuals of *Sobrarbesiren*, the temporal crests are present on both the frontal and the parietal (Fig. 4). However, the temporal crests are present on the parietal of the MPZ 2020/598 juvenile, but they are absent on all the isolated frontals recovered from perinatals to juveniles (Fig. 5). Thus, there is perhaps a different pattern of ontogenetic development of the temporal crests in *Sobrarbesiren* compared with '*Halitherium*' *taulannense*. Nevertheless, more complete juvenile skulls are necessary to confirm this hypothesis.

With respect to the frontals, another ontogenetic variation is in the grade of development of the supraorbital process, which is almost absent in the perinatal individuals MPZ 2020/592 and MPZ 2020/594 but already present in the specimens MPZ 2020/593 and MPZ 2020/595 assigned to juvenile individuals (Fig. 5). In addition, the posterolateral borders of the supraorbital processes of the juvenile frontals are diagonal with respect to the midline of the frontals, whereas they are more perpendicular in the subadult–young adult skulls, as observed in *Trichechus* spp. (Domning & Hayek, 1986). Furthermore, the bulge and the cord-like protuberances present on

the posterolateral side of the supraorbital process of the frontal in the subadult–young adult individuals are incipient in MPZ 2020/593 and MPZ 2020/595, whereas they are absent in MPZ 2020/592 and MPZ 2020/594; hence, it seems that these ornamentations appear during ontogenetic development.

Variations in the angle formed by the supraoccipital with the posterior part of the parietals have been observed in fossil sirenians (e.g. 99–126° in *Metaxytherium floridanum*, Domning, 1988; 109–123° in *Metaxytherium serresii* Carone *et al.*, 2013; 120–140° in *Kaupitherium gruelli* Voss & Hampe, 2017) but were not postulated to represent either ontogenetic development or sexual dimorphism. The angle formed by the supraoccipital with the posterior part of the parietals in *Sobrarbesiren* varies from 100 to 138° (Supporting Information, Table S2; An SO-P), being higher in the juvenile skullcaps MPZ 2020/598–599 than in the subadult–young adult type skulls; hence, this angle probably diminishes during the growth of the animal to maturity. Nevertheless, more specimens are necessary to corroborate this assumption.

Another common intraspecific variation observed in sirenians is the presence/absence of emissary foramina. This variation has been described in '*Halitherium*' *taulannense*, *Protosiren* sp., *Metaxytherium floridanum*, *Dusisiren jordani* Kellogg, 1925 and *Nanosiren garciae* Domning & Aguilera, 2008 (Domning, 1978, 1988; Domning *et al.*, 1982; Sagne, 2001a; Domning & Aguilera, 2008), without any ontogenetic or sexual constraint. With respect to Holocene sirenians, *Hydrodamalis gigas* and *Dugong dugon* possess an emissary foramen in the parietal bone, whereas it is absent in *Trichechus* (according to Kaiser, 1974). Nevertheless, personal observations (E.D.B.) of *Trichechus manatus* skulls also indicate variations in the presence (MNHN 1921-122) or absence (MB.MA. 48858) of the emissary foramen in this taxon. In *Sobrarbesiren*, emissary foramina are present only in the skull roof of the holotype skull *MPZ 2017/1* (Fig. 4C).

Palaeoecology

Sirenians show varying degrees of rostral deflection, which are related to the degree of specialization for bottom feeding (Domning, 1977b). *Sobrarbesiren* shows a downturned snout, supporting the idea that it specialized in feeding on aquatic bottom plants, albeit in relatively low degree (32°) by comparison with non-prorastomid Eocene sirenians (see Discussion above). In comparison with extant sirenians, the degree of rostral deflection of *Sobrarbesiren* falls within the range of variability of extant trichechids (25–50°), which feed on both fluvial and marine vegetation (Domning & Hayek, 1986), and diverges from the extremely downturned snout of *Dugong dugon* (70°; Domning, 2001b), which feeds exclusively on seagrasses except in extreme situations (Marsh *et al.*, 2018). Furthermore, it has been proposed that in their transition from a land habitat to marine environments, pan-sirenians such as 'prorastomids' probably exploited freshwater plants as feeding resources before acquiring a seagrass-based diet (Savage *et al.*, 1994; Domning, 2001b). 'Prorastomids' have been found associated with coastal river deposits (Savage *et al.*, 1994; Domning, 2001a) in a similar way to *Sobrarbesiren*, which was found in a deltaic plain deposit (Díaz-Berenguer *et al.*, 2018). In contrast, other Eocene pan-sirenians, including protosirenids, are associated with open-sea depositional environments (e.g. Domning & Gingerich, 1994; Gingerich *et al.*, 1995; Sagne, 2001a; Zalmout *et al.*, 2003; Samonds *et al.*, 2009; Zalmout & Gingerich, 2012; Balaguer & Alba, 2016; Domning *et al.*, 2017). Nevertheless, regardless of the depositional environment, isotopic data show that seagrasses were already the main component of the diet of basal sirenians, such as 'prorastomids', protosirenids and other Eocene genera (Clementz *et al.*, 2009; Clementz & Sewall, 2011: table S1). The existence of seagrasses in the Ainsa Basin during the Eocene is confirmed by the presence of certain species of benthonic foraminifera associated with this type of angiosperm (Mateu-Vicens *et al.*, 2012). Therefore, seagrasses were probably the main component of the diet of *Sobrarbesiren*.

Domning (2001b) proposes that a narrow rostrum and a narrow mandibular symphysis in Eocene pan-sirenians are indicative of selective browsers. Although the morphology of the *Sobrarbesiren* mandible is unknown, its rostrum is narrow (Fig. 2), as in 'prorastomids' and other Eocene sirenians that probably had diets based on bottom-growing and floating aquatic plants combined (Savage *et al.*, 1994; Domning, 2001b). In contrast, protosirenids, which possess a broad rostrum, were probably indiscriminate grazers (Domning, 2001b; Domning *et al.*, 2017). *Sobrarbesiren* probably fed mainly in shallow coastal waters and was a selective browser, with a diet based mainly on seagrasses and perhaps some floating plants.

With regard to the ear region, the tympanic membrane of extant sirenians inserts into the inner surface of the posterior arm, and into the ventral border of the tympanic arch, filling it (Robineau, 1969; Ketten *et al.*, 1992). Therefore, the diameter of the tympanic arch might reflect the size of this membrane. Chapla *et al.* (2007) proposed that the large tympanic membrane of extant *Trichechus manatus latirostris* Harlan, 1824 might be an adaptation to the longer wavelengths of sound in subaquatic environments than in air. According to Ketten *et al.* (1992), morphofunctional changes in the middle ear of pan-sirenians from the Eocene to present-day taxa are scarce. Nevertheless, the smaller diameter of

the tympanic arch observed in stem pan-sirenians, such as *Prorastomus* and *Sobrarbesiren*, in contrast to other Eocene and post-Eocene sirenians implies a smaller tympanic membrane and can be considered a preliminary indication of an ear less evolved for hearing under the water. Thus, a relationship between the size of the tympanic arch and the aquatic adaptation of sirenians cannot be ruled out.

CONCLUSIONS

The study of the new cranial elements assigned to *Sobrarbesiren cardieli* from the middle Eocene (Lutetian) of Huesca Province (Spain) has shed new light on the skull osteology of this stem pan-sirenian. *Sobrarbesiren* presents a combination of plesiomorphic and apomorphic characters. The studied specimens, which pertain to eight different individuals ranging from perinatal to young adults, do not show significant intraspecific variation except in the development of the temporal crests, as proposed for other fossil pan-sirenians. Variations in the angle formed by the supraoccipital with the posterior part of the parietals and in the structures of the frontal bone are probably related to ontogenetical development, with the latter also observed in extant *Trichechus* spp.

The palaeoecological study of the cranial elements indicates that *Sobrarbesiren* was a selective browser that fed mainly on seagrasses in shallow coastal waters, probably combined with some floating plants. Furthermore, the morphology of the tympanic bone might provide a clue to understanding the adaptations of the ear region of sirenians to aquatic life, revealing that the middle ear of *Sobrarbesiren* was not adapted totally to life in water.

In our phylogenetic analysis, *Sobrarbesiren* is recovered as the internal specifier of a new clade containing *Sobrarbesiren cardieli* plus the taxa *Eotheroides aegyptiacum*, *Prototherium veronense* and *Prototherium ausetanum*. This is the sister clade of the rest of the pan-sirenians except the 'prorastomids'; hence, the position of *Sobrarbesiren* as a basal stem pan-sirenian is maintained.

Our phylogenetic analysis supports the idea that the inclusion of characters relating to the endocranium and the basioccipital bone in the character matrix can prove useful to resolving the phylogenetic relationships of stem Pan-Sirenia. The six new characters added (Ch.223–228) not only increase the resolution of the consensus topology, but also provide further support for previously established clades. In addition, we confirm that the absence of endocranial structures is not diagnostic for Protosirenidae, but the plesiomorphic condition for pan-sirenians. Our results show that anatomical and phylogenetic studies of Eocene stem pan-sirenians are far from finished and that detailed studies on new and old taxa, together with the implementation of more sophisticated phylogenetic tools, are sure to shake the topology of the stem.

ACKNOWLEDGEMENTS

We thank C. Sagne (Muséum national d'Histoire naturelle, Paris), P. Brewer (Natural History Museum, London), M. G. Fornasiero (Museum of Geology and Paleontology, University of Padua, Padua), Thomas Schossleitner (Museum für Naturkunde, Berlin) and especially D. Domning (Smithsonian Institution National Museum of Natural History, Washington, DC) for his advice and comments during our stay in Washington, DC. We thank Alexandra Fernandez (NOVA School of Sciences and Tecnology) for her help in finding the bibliography.

FUNDING

Financial support was provided by the Ministerio de Economía y Competitividad (CGL2013-47521-P) and by the Ministerio de Ciencia e Innovación (CGL2017-85038-P, Ministerio de Economía y Competitividad/ Fondo Europeo de Desarrollo Regional, Unión Europea, UE), the Research Groups of the Gobierno Vasco/Eusko Jaurlaritza (IT834-13, IT1004-16 and IT418-19), the Universidad del País Vasco/ Euskal Herriko Unibertsitatea (PPG17/04 and GIU18/ 163), the Geoparque de Sobrarbe, the European Regional Development Fund, the Government of Aragón ('DGA' and 'Grupos de Referencia' E18_17R) and grant UIDB/04035/2020 from the Fundação para a Ciência e a Tecnologia (GeoBioTec, GeoBioCiências, GeoTecnologias e GeoEngenharias). M.M.-A. is supported by the Fundação para a Ciência e a Tecnologia (grant number SFRH/ BPD/ 113130/ 2015). R. Glasgow edited the English. We thank the anonymous reviewer and the Editor, Dr Maarten Christenhusz, for their comments, which greatly improved our manuscript.

DATA AVAILABILITY

All available data is given in the supporting information of this paper. The dataset used in this study can be downloaded from Morphobank (http://morphobank.org/permalink/?P3923).

REFERENCES

Abel O. 1907. Die Stammesgeschichte der Meeressäugetiere. *Meereskunde* **1:** 1–36.

Abel O. 1913. Die eocänen Sirenen der Mittelmeerregion. I. Teil: der Schädel von *Eotherium aegyptiacum*. *Palaeontographica* **59:** 289–360.

Abel O. 1928. Vorgeschichte der Sirenia. *Zweite Auflage*. In: Weber M ed. *Die Säugetiere, Einfürung in die Anatomie und Systematik der recenten und fossilen Mammalia*. Jena: Gustav Fischer, 496–504.

Amrine-Madsen H, **Koepfli KP**, **Wayne RK**, **Springer MS. 2003.** A new phylogenetic marker, apolipoprotein B, provides compelling evidence for eutherian relationships. *Molecular Phylogenetics and Evolution* **28:** 225–240.

Aranda-Manteca FJ, **Domning DP**, **Barnes LG. 1994.** A new Middle Miocene sirenian of the genus *Metaxytherium* from Baja California and California: relationships and paleobiogeographic implications. *Proceedings of the San Diego Society of Natural History* **29:** 191–204.

Asher RJ, **Novacek MJ**, **Geisler JH. 2003.** Relationships of endemic African mammals and their fossil relatives based on morphological and molecular evidence. *Journal of Mammalian Evolution* **10:** 131–194.

Bajpai S, **Domning DP. 1997.** A new dugongine sirenian from the early Miocene of India. *Journal of Vertebrate Paleontology* **17:** 219–228.

Bajpai S, **Domning DP**, **Das DP**, **Mishra VP. 2009.** A new middle Eocene sirenian (Mammalia, Protosirenidae) from India. *Neues Jahrbuch für Geologie und Paläontologie - Abhand* **11:** 257–267.

Balaguer J, **Alba DM. 2016.** A new dugong species (Sirenia, Dugongidae) from the Eocene of Catalonia (NE Iberian Peninsula). *Comptes Rendus Palevol* **15:** 489–500.

Bizzotto B. 1983. *Prototherium intermedium* n. sp. (Sirenia) dell'Eocene superiore di Possagno e proposta di revisione sistematica del taxon *Eotheroides* Palmer 1899. *Memorie degli Istituti di Geologia e Mineralogia dell'Università di Padova* **36:** 95–116.

Carone G, **Domning DP. 2007.** *Metaxitherium serresii* (Mammalia: Sirenia): new pre-Pliocene record, and implications for Mediterranean paleoecology before and after the Messinian Salinity Crisis. *Bollettino della Società Paleontologica Italiana* **46:** 55–92.

Carone G, **Domning DP**, **Marra AC. 2013.** New finds of *Metaxytherium serresii* (Gervais, 1847) (Mammalia: Sirenia) from the Upper Miocene of Monte Poro (Calabria, Italy). *Bollettino della Società Paleontologica Italiana* **52:** 187–196.

Chapla ME, **Nowacek DP**, **Rommel SA**, **Sadler VM. 2007.** CT scans and 3D reconstructions of Florida manatee (*Trichechus manatus latirostris*) heads and ear bones. *Hearing Research* **228:** 123–135.

Clementz MT, **Sewall JO. 2011.** Latitudinal gradients in greenhouse seawater ^{18}O: evidence from Eocene sirenian tooth enamel. *Science* **332:** 455–458.

Clementz MT, **Sorbi S**, **Domning DP. 2009.** Evidence of Cenozoic environmental and ecological change from stable isotope analysis of sirenian remains from the Tethys-Mediterranean region. *Geology* **37:** 307–310.

Cope ED. 1883. On a new extinct genus of Sirenia, from South Carolina. *Proceedings of the Academy of Natural Sciences of Philadelphia* **35:** 52–54.

Delfortrie E. 1872. Étude sur les restes fossiles de siréniens du genre '*Halitherium*', dans le bassin de la Garonne. *Actes de la Société Linnéenne de Bordeaux* **28:** 281–324.

Díaz-Berenguer E, **Badiola A**, **Moreno-Azanza M**, **Canudo JI. 2018.** First adequately-known quadrupedal sirenian from Eurasia (Eocene, Bay of Biscay, Huesca, northeastern Spain). *Scientific Reports* **8:** 5127.

Díaz-Berenguer E, **Houssaye A**, **Badiola A**, **Canudo JI. 2020.** The hind limbs of *Sobrarbesiren cardieli* (Eocene, northeastern Spain) and new insights into the locomotion capabilities of the quadrupedal sirenians. *Journal of Mammalian Evolution* **27:** 649–675.

Domning DP. 1977a. Observations on the myology of *Dugong dugon* (Müller). *Smithsonian Contributions to Zoology* **226:** 1–55.

Domning DP. 1977b. An ecological model for Late Tertiary sirenian evolution in the North Pacific Ocean. *Systematic Zoology* **25:** 352–362.

Domning DP. 1978. Sirenian evolution in the North Pacific Ocean. *University of California Publications in Geological Sciences* **118:** 1–179.

Domning DP. 1988. Fossil Sirenia of the West Atlantic and Caribbean region. I. *Metaxytherium floridanum* Hay, 1922. *Journal of Vertebrate Paleontology* **8:** 395–426.

Domning DP. 1989. Fossil Sirenia of the West Atlantic and Caribbean Region. II. *Dioplotherium manigaulti* Cope, 1883. *Journal of Vertebrate Paleontology* **9:** 415–428.

Domning DP. 1994. A phylogenetic analysis of the Sirenia. *Proceedings of the San Diego Society of Natural History* **29:** 177–189.

Domning DP. 1996. Bibliography and index of the Sirenia and Desmostylia. *Smithsonian Contributions to Paleobiology* **80:** 1–611.

Domning DP. 2001a. The earliest known fully quadrupedal sirenian. *Nature* **413:** 625–627.

Domning DP. 2001b. Sirenians, seagrasses, and Cenozoic ecological change in the Caribbean. *Palaeogeography, Palaeoclimatology, Palaeoecology* **166:** 27–50.

Domning DP, **Aguilera OA. 2008.** Fossil Sirenia of the West Atlantic and Caribbean region. VIII. *Nanosiren garciae*, gen. et sp. nov. and *Nanosiren sanchezi*, sp. nov. *Journal of Vertebrate Paleontology* **28:** 479–500.

Domning DP, **Gingerich PD. 1994.** *Protosiren smithae*, new species (Mammalia, Sirenia) from the late middle Eocene of Wadi Hitan, Egypt. *Contributions from the Museum of Paleontology University of Michigan* **29:** 69–87.

Domning DP, **Hayek LAC. 1986.** Interspecific and intraspecific morphological variation in manatees (Sirenia: *Trichechus*). *Marine Mammal Science* **2:** 87–144.

Domning DP, **Heal GJ**, **Sorbi S. 2017.** *Libysiren sickenbergi*, gen. et sp. nov.: a new sirenian (Mammalia, Protosirenidae) from the middle Eocene of Libya. *Journal of Vertebrate Paleontology* **37:** e1299158.

Domning DP, **Morgan GS**, **Ray CE. 1982.** North American Eocene sea cows (Mammalia: Sirenia). *Smithsonian Contributions to Paleobiology* **52:** 1–69.

Domning DP, **Pervesler P. 2001.** The osteology and relationships of *Metaxytherium krahuletzi* Depéret, 1895

(Mammalia: Sirenia). *Abhandlungen der Senckenbergischen Naturforschenden Gesellschaft* **553:** 1–89.

Domning DP, **Sorbi S. 2011.** *Rytiodus heali*, sp. nov., a new sirenian (Mammalia, Dugonginae) from the Miocene of Libya. *Journal of Vertebrate Paleontology* **31:** 1338–1355.

Edinger T. 1933. Ergebnisse der Forschungsreisen Prof. E. Stromers in den Wüsten Ägyptens. V. Tertiäre Wirbeltiere. 5. Über Gehirne tertiärer Sirenia Ägyptens und Mitteleuropas sowie der rezenten Seekühe. *Abhandlungen der Bayerischen Akademie der Wissenschaften. Mathematisch-naturwissenschaftliche Abteilung* **20:** 1–36.

Furusawa H. 2004. A phylogeny of the North Pacific Sirenia (Dugongidae: Hydrodamalinae) based on a comparative study of endocranial casts. *Paleontological Research* **8:** 91–98.

Gheerbrant E, **Domning DP**, **Tassy P. 2005.** Paenungulata (Sirenia, Proboscidea, Hyracoidea, and relatives). In: Rose KD, Archibald JD eds. *The rise of placental mammals: origins and relationships of the major extant clades*. Baltimore: Johns Hopkins University Press, 84–105.

Gheerbrant E, **Sudre J**, **Cappetta H. 1996.** A Palaeocene proboscidean from Morocco. *Nature* **383:** 68–70.

Gingerich PD, **Arif M**, **Akram Bhatti M**, **Raza HA**, **Mahmood Raza S. 1995.** *Protosiren* and *Babiacetus* (Mammalia, Sirenia and Cetacea) from the middle Eocene Drazinda Formation, Sulaiman Range, Punjab (Pakistan). *Contributions from the Museum of Paleontology University of Michigan* **29:** 331–357.

Gingerich PD, **Domning DP**, **Blane CE**, **Uhen MD. 1994.** Cranial morphology of *Protosiren fraasi* (Mammalia, Sirenia) from the middle Eocene of Egypt: a new study using computed tomography. *Contributions from the Museum of Paleontology University of Michigan* **29:** 41–67.

Goloboff PA. 2014. Extended implied weighting. *Cladistics* **30:** 260–272.

Goloboff PA, **Catalano SA. 2016.** TNT version 1.5, including a full implementation of phylogenetic morphometrics. *Cladistics* **32:** 221–238.

Hay OP. 1922. Description of a new fossil sea cow from Florida, *Metaxytherium floridanum*. *Proceedings of the United States National Museum* **61:** 1–4.

Kaiser HE. 1974. *Morphology of the Sirenia. A macroscopic and X-ray atlas of the osteology of recent species*. Basel: Karger Publishers.

Kellogg R. 1925. A new fossil sirenian from Santa Barbara County, California. *Carnegie Institution of Washington* **348:** 9–11.

Ketten DR, **Odell DK**, **Domning DP. 1992.** Structure, function, and adaptation of the manatee ear. In: Thomas JA, Kastelein RA, Supin AY, eds. *Marine mammal sensory systems*. Boston: Springer US, 77–95.

Marsh H, **Grech A**, **McMahon K. 2018.** Dugongs: seagrass community specialists. In: Larkum AWD, Kendrick GA, Ralph PJ, eds. *Seagrasses of Australia: structure, ecology and conservation*. Cham: Springer International, 629–661.

Mateu-Vicens G, **Pomar L**, **Ferràndez-Cañadell C. 2012.** Nummulitic banks in the upper Lutetian 'Buil level', Ainsa Basin, South Central Pyrenean Zone: the impact of internal waves. *Sedimentology* **59:** 527–552.

McKenna MC. 1975. Toward a phylogenetic classification of the Mammalia. In: Luckett WP, Szalay FS, eds. *Phylogeny of the primates: a multidisciplinary approach*. Boston: Springer US, 21–46.

Mitchell J. 1973. Determination of relative age in the dugong *Dugong dugon* (Müller) from a study of skulls and teeth. *Zoological Journal of the Linnean Society* **53:** 1–23.

Murphy WJ, **Pevzner PA**, **O'Brien SJ. 2004.** Mammalian phylogenomics comes of age. *Trends in Genetics* **20:** 631–639.

Nojima T. 1988. Developmental pattern of the bony falx and bony tentorium of spotted dolphins (*Stenella attenuata*) and the relationship between degree of development and age. *Marine Mammal Science* **4:** 312–322.

Nojima T. 1990. The relationship between development of the bony falx and bony tentorium in cetaceans and their diets. *Scientific Reports of the Whales Research Institute* **1:** 39–61.

O'Leary MA, **Bloch JI**, **Flynn JJ**, **Gaudin TJ**, **Giallombardo A**, **Giannini NP**, **Goldberg SL**, **Kraatz BP**, **Luo Z-X**, **Meng J**, **Ni X**, **Novacek MJ**, **Perini FA**, **Randall ZS**, **Rougier GW**, **Sargis EJ**, **Silcox MT**, **Simmons NB**, **Spaulding M**, **Velazco PM**, **Weksler M**, **Wible JR**, **Cirranello AL. 2013.** The placental mammal ancestor and the post-K-Pg radiation of placentals. *Science* **339:** 662–667.

Orihuela J, **López LWV**, **Macrini TE. 2019.** First cranial endocasts of early Miocene sirenians (Dugongidae) from the West Indies. *Journal of Vertebrate Paleontology* **39:** e1584565.

Ozawa T, **Hayashi S**, **Mikhelson VM. 1997.** Phylogenetic position of mammoth and Steller's sea cow within Tethytheria demonstrated by mitochondrial DNA sequences. *Journal of Molecular Evolution* **44:** 406–413.

Pardini AT, **O'Brien PCM**, **Fu B**, **Bonde RK**, **Elder FFB**, **Ferguson-Smith MA**, **Yang F**, **Robinson TJ. 2007.** Chromosome painting among Proboscidea, Hyracoidea and Sirenia: support for Paenungulata (Afrotheria, Mammalia) but not Tethytheria. *Proceedings of the Royal Society B: Biological Sciences* **274:** 1333–1340.

Pilleri G. 1987. *The Sirenia of the Swiss Molasse: with a descriptive catalogue of the fossil Sirenia preserved in Swiss collections*. Ostermundigen: Brain Anatomy Institute, University of Berne.

Pilleri G, **Biosca J**, **Via L. 1989.** *The Tertiary Sirenia of Catalonia*. Ostermundingen: Brain Anatomy Institute, University of Berne.

Pocock RI. 1940. Some notes on the dugong. *Annals and Magazine of Natural History* **5:** 329–345.

Robineau D. 1969. Morphologie externe du complexe osseux temporal chez les sireniens. *Éditions du Muséum National de Histoire Naturelle* **IX:** 1–32.

Sagne C. 2001a. *La diversification des siréniens à l'Eocène (Sirenia, Mammalia): étude morphologique et analyse phylogénétique du sirénien de Taulanne,* Halitherium taulannense. Unpublished D. Phil. Thesis, Muséum National d'Histoire Naturelle, Paris.

Sagne C. 2001b. *Halitherium taulannense*, nouveau sirénien (Sirenia, Mammalia) de l'Éocène supérieur provenant du domaine Nord-Téthysien (Alpes-de-Haute-Provence,

France). *Comptes Rendus de l'Académie des Sciences - Series IIA - Earth and Planetary Science* **333:** 471–476.

Samonds KE, **Zalmout IS**, **Irwin MT**, **Krause DW**, **Rogers RR**, **Raharivony LL. 2009.** *Eotheroides lambondrano*, new middle Eocene sea cow (Mammalia, Sirenia) from the Mahajanga Basin, northwestern Madagascar. *Journal of Vertebrate Paleontology* **29:** 1233–1243.

Savage RJ. 1976. Review of early Sirenia. *Systematic Zoology* **25:** 344–351.

Savage RJG, **Domning DP**, **Thewissen JGM. 1994.** Fossil Sirenia of the west Atlantic and Caribbean region. V. The most primitive known sirenian, *Prorastomus sirenoides* Owen, 1855. *Journal of Vertebrate Paleontology* **14:** 427–449.

Seiffert ER. 2007. A new estimate of afrotherian phylogeny based on simultaneous analysis of genomic, morphological, and fossil evidence. *BMC Evolutionary Biology* **7:** 224.

Sickenberg O. 1934. Beiträge zur Kenntnis Tertiärer Sirenen. I. Die eozänen Sirenen des Mittelmeergebietes. II. Die Sirenen des Belgischen Tertiärs. *Mémoires du Musée Royal d'Histoire Naturelle de Belgique* **63:** 1–352.

Siegfried P. 1965. *Anomotherium langewieschei* n. g. n. sp. (Sirenia) aus dem Ober-Oligozän des Dobergs bei Bünde (Westfalen). *Palaeontographica Abteilung A Band* **A124:** 116–150.

Simpson GG. 1945. Principles of classification and a classification of mammals. *Bulletin of the American Museum of Natural History* **85:** 1–350.

Sorbi S, **Domning DP**, **Vaiani SC**, **Bianucci G. 2012.** *Metaxytherium subapenninum* (Bruno, 1839) (Mammalia, Dugongidae), the latest sirenian of the Mediterranean Basin. *Journal of Vertebrate Paleontology* **32:** 686–707.

Springer MS, **Murphy WJ. 2007.** Mammalian evolution and biomedicine: new views from phylogeny. *Biological Reviews of the Cambridge Philosophical Society* **82:** 375–392.

Springer MS, **Signore AV**, **Paijmans JLA**, **Vélez-Juarbe J**, **Domning DP**, **Bauer CE**, **He K**, **Crerar L**, **Campos PF**, **Murphy WJ**, **Meredith RW**, **Gatesy J**, **Willerslev E**, **MacPhee RDE**, **Hofreiter M**, **Campbell KL. 2015.** Interordinal gene capture, the phylogenetic position of Steller's sea cow based on molecular and morphological data, and the macroevolutionary history of Sirenia. *Molecular Phylogenetics and Evolution* **91:** 178–193.

Tabuce R, **Asher RJ**, **Lehmann T. 2008.** Afrotherian mammals: a review of current data. *Mammalia* **72:** 2–14.

Thewissen JGM, **Bajpai S. 2009.** A new Miocene sirenian from Kutch, India. *Acta Palaeontologica Polonica* **54:** 7–13.

Vélez-Juarbe J, **Domning DP. 2014.** Fossil Sirenia of the West Atlantic and Caribbean region. IX. *Metaxytherium albifontanum*, sp. nov. *Journal of Vertebrate Paleontology* **34:** 444–464.

Vélez-Juarbe J, **Domning DP. 2015.** Fossil Sirenia of the West Atlantic and Caribbean region. XI. *Callistosiren boriquensis*, gen. et sp. nov. *Journal of Vertebrate Paleontology* **35:** e885034.

Velez-Juarbe J, **Domning DP**, **Pyenson ND. 2012.** Iterative evolution of sympatric sea cow (Dugongidae, Sirenia) assemblages during the past ~26 million years. *PLoS One* **7:** e31294.

Velez-Juarbe J, **Wood AR. 2018.** An early Miocene dugongine (Sirenia: Dugongidae) from Panama. *Journal of Vertebrate Paleontology* **38:** e1511799.

Voss M, **Hampe O. 2017.** Evidence for two sympatric sirenian species (Mammalia, Tethytheria) in the early Oligocene of Central Europe. *Journal of Paleontology* **91:** 337–367.

Zalmout IS, **Gingerich PD. 2012.** Late Eocene seacows (Mammalia, Sirenia) from Wadi Al Hitan in the western desert of Fayum, Egypt. *University of Michigan Papers on Paleontology* **387:** 1–158.

Zalmout IS, **Ul-Haq M**, **Gingerich PD. 2003.** New species of *Protosiren* (Mammalia, Sirenia) from the early middle Eocene of Balochistan (Pakistan). *Contributions from the Museum of Paleontology University of Michigan* **31:** 79–87.

SUPPORTING INFORMATION

Additional Supporting Information may be found in the online version of this article at the publisher's web-site:

Table S1. List of taxa included in the phylogenetic analysis, and references and specimens used for the coding of characters 223–228.
Table S2. Measurements of skulls and skull fragments of *Sobrarbesiren cardieli*.
Table S3. Measurements of the tympanic bone of various sirenians.
Table S4. Measurements of the upper dentition of *Sobrarbesiren cardieli*.
File S1. TNT file with the dataset and settings used for the cladistic analysis.
Figure S1. Strict consensus tree of the 7560 most parsimonious trees.
Figure S2. Strict consensus tree of the 945 most parsimonious trees under implied weighting analysis.
Figure S3. Implied weighting analysis consensus tree with a parsimony-based character reconstruction of character 223.
Figure S4. Implied weighting analysis consensus tree with a parsimony-based character reconstruction of character 224.
Figure S5. Implied weighting analysis consensus tree with a parsimony-based character reconstruction of character 225.
Figure S6. Implied weighting analysis consensus tree with a parsimony-based character reconstruction of character 226.

Figure S7. Implied weighting analysis consensus tree with a parsimony-based character reconstruction of character 227.
Figure S8. Implied weighting analysis consensus tree with a parsimony-based character reconstruction of character 228.